

~~CONFIDENTIAL~~

Copy 7  
RM E55K01

NACA RM E55K01

UNCLASSIFIED

NACA

# RESEARCH MEMORANDUM

ZERO-ANGLE-OF-ATTACK PERFORMANCE OF TWO-DIMENSIONAL

INLETS NEAR MACH NUMBER 3

By Richard R. Woollett and James F. Connors

Lewis Flight Propulsion Laboratory  
Cleveland, Ohio

FOR REFERENCE

NOT TO BE TAKEN FROM THIS ROOM

CLASSIFIED DOCUMENT

This material contains information affecting the National Defense of the United States within the meaning of the espionage laws, Title 18, U.S.C., Secs. 793 and 794, the transmission or revelation of which in any manner to an unauthorized person is prohibited by law.

NATIONAL ADVISORY COMMITTEE  
FOR AERONAUTICS

WASHINGTON  
February 29, 1956

CLASSIFICATION CHANGED

UNCLASSIFIED

To

By author

Date 2/10/60

J.F.H. #17

~~CONFIDENTIAL~~

UNCLASSIFIED



UNCLASSIFIED

## TABLE OF CONTENTS

	Page
SUMMARY . . . . .	1
INTRODUCTION . . . . .	1
APPARATUS AND PROCEDURE . . . . .	2
Models . . . . .	2
Compression surfaces . . . . .	3
Subsonic diffusers . . . . .	3
Side plates . . . . .	4
Instrumentation . . . . .	4
RESULTS . . . . .	5
Effects of Compression Surface on Performance . . . . .	6
Pressure recovery and mass-flow characteristics . . . . .	6
Inlet stability characteristics . . . . .	6
Visual flow observations . . . . .	7
Effects of Subsonic Diffuser on Performance . . . . .	10
Pressure recovery and mass-flow characteristics . . . . .	10
Inlet stability . . . . .	11
Visual flow observations . . . . .	12
Effects of Side Plate on Performance . . . . .	13
Pressure recovery and mass-flow characteristics . . . . .	13
Inlet stability . . . . .	13
Visual flow observations . . . . .	13
DISCUSSION . . . . .	14
SUMMARY OF RESULTS . . . . .	15
REFERENCES . . . . .	16
TABLES	
I - SUBSONIC-DIFFUSER CONFIGURATIONS . . . . .	18
II - EFFECT OF COMPRESSION SURFACE ON PERFORMANCE . . . . .	19
III - EFFECT OF SUBSONIC DIFFUSER ON PERFORMANCE . . . . .	20
IV - EFFECT OF SIDE PLATE ON PERFORMANCE . . . . .	21

UNCLASSIFIED

## NATIONAL ADVISORY COMMITTEE FOR AERONAUTICS

RESEARCH MEMORANDUMZERO-ANGLE-OF-ATTACK PERFORMANCE OF TWO-DIMENSIONAL  
INLETS NEAR MACH NUMBER 3

By Richard R. Woollett and James F. Connors

## SUMMARY

An extensive program was undertaken to investigate the effect of several geometric variables on the performance of two-dimensional inlets. This investigation included inlets having single-wedge, double-wedge, and isentropic compression ramps with various side-plate configurations and subsonic diffusers. The tests were conducted over a range of Reynolds number based on inlet height from 0.50 to  $2.67 \times 10^6$ . Generally, the performance levels of the two-dimensional inlets were somewhat below those obtained previously with comparable axisymmetric models. At Mach number 3.05 the optimum total-pressure recovery was obtained with an isentropic inlet which compressed the external flow to a Mach number of 1.88. Rectangular side plates and a long high-exit-Mach-number subsonic diffuser with filleted corners were used with this inlet. A critical total-pressure recovery of 0.71 was realized with a corresponding mass-flow ratio of 0.965. Subcritical stability to a mass-flow ratio of 0.60 was obtained.

The following general observations were made with regard to the relative effects of the test variables upon inlet performance: (1) Pressure recovery generally increased in the following order for the supersonic compression surfaces investigated: single wedge (0.41), 2.10 isentropic (0.58), double wedge (0.605), 1.55 isentropic (0.65), and 1.88 isentropic (0.71); (2) long faired subsonic diffusers with an average angle of divergence of  $4^\circ$  gave an increase in pressure recovery of approximately 0.05 over that for the short diffuser with an average angle of divergence of  $10^\circ$ ; (3) although pressure recovery and mass flow were reduced with the use of short side plates, the range of stable subcritical operation was somewhat extended; and (4) for the range investigated, Reynolds number generally had little or no effect upon inlet performance. In no case did the addition of leading-edge roughness improve performance.

## INTRODUCTION

Preliminary investigations have been conducted by the NACA to evaluate the performance capabilities of two-dimensional inlets at Mach

numbers of 3 and above. Such inlets generally find application as wing-leading-edge installations or as side inlets with full boundary-layer removal. Previous work at Mach number 3.85 (ref. 1) demonstrated that twin-duct arrangements of these inlets incur large (perhaps intolerable) discontinuities in performance between subcritical and supercritical operation with pronounced hysteresis. In order to avoid this difficulty, single-passage configurations were used throughout the present investigation.

The aim of this study at the NACA Lewis laboratory was to determine systematically the performance characteristics of single-passage two-dimensional inlets with either single-oblique-shock, double-oblique-shock, or isentropic compression surfaces. (The single-oblique-shock and double-oblique-shock inlets are hereinafter referred to as single-wedge and double-wedge inlets, respectively.) The effects on inlet performance of Reynolds number, internal ducting (such as rate of divergence and corner filleting), and external side-plate configuration were also investigated. Glass side plates provided the added benefit of flow visualization not possible with three-dimensional models and permitted a better study of the flow problems common to both two-dimensional and axisymmetric inlets.

Each inlet was designed to achieve high performance for its particular type of compression surface with low external drag. Performance was evaluated in terms of pressure recovery, mass flow, and exit total-pressure profiles. The investigation was conducted at zero angle of attack.

#### APPARATUS AND PROCEDURE

Most of the experimental work was conducted in the Lewis 18- by 18-inch supersonic tunnel at Mach number 3.05 and a simulated pressure altitude of 80,000 feet. The tunnel air was maintained at a stagnation temperature of  $150^{\circ}\text{F}$  and a dew-point temperature of  $-15^{\circ}\pm 5^{\circ}\text{F}$ . Based upon the maximum height of the inlet (4 in.), the Reynolds number was  $0.5\times 10^6$ .

In order to determine the effects of Reynolds number and leading-edge roughness (1/2-in. strip of no. 60 carborundum grit), tests were also conducted in the Lewis 1- by 1-foot variable Reynolds number tunnel at a Mach number of 3.12, where the Reynolds number based upon the maximum height of the inlet (4 in.) was varied from 0.50 to  $2.67\times 10^6$ . The simulated pressure altitude for this tunnel varied from 30,000 to 80,000 feet. The air was maintained at a stagnation temperature of approximately  $70^{\circ}\text{F}$  and a dew-point temperature of  $-50^{\circ}\pm 5^{\circ}\text{F}$ .

#### Models

The model installation with one glass side plate removed is shown in figure 1(a). The supports located on the external surface of the

cowl were necessary to prevent a distortion of the thin leading-edge surface. These supports were designed with a sharp leading edge so that there would be no interference with the entrance flow. The sonic discharge area was varied by means of a movable plug, which is shown in figure 1(b).

Compression surfaces. - Three types of compression surface were studied; namely, single wedge, double wedge, and isentropic ramps (fig. 1(c)). The initial angle ( $19^\circ$ ) of the single-wedge inlet with near-maximum allowable internal contraction corresponded to that for maximum theoretical pressure recovery. The cowl of this inlet was designed so that the internal lip shock was  $3^\circ$  less than the local detachment angle. The resultant cowl shape had a small frontal area and should result in near-minimum cowl pressure drag.

The design pressure recovery of a double-wedge inlet with internal contraction was similarly optimized with resulting wedge angles of  $10^\circ$  and  $25^\circ$ . A low-drag lip contoured in a manner similar to the cowl of the single-wedge inlet was used.

Three isentropic compression ramps were used to compress the external flow to various Mach numbers. These isentropic inlets, each having an initial wedge angle of  $6^\circ$ , were so designed that the internal cowl-lip angle was  $3^\circ$  less than the local detachment angle (with the exception of the 1.55-isentropic inlet). By constructing the characteristics of the internal flow, the local turning of the cowl surface was designed so that the local-flow Mach number would not be less than 1.2, with consideration, of course, of the effect of expansion waves from the shoulder of the compression wedge (see fig. 2). Because of the near-maximum strength of the internal lip shock, which compresses the flow nearly to this limit, no internal compressive turning along the cowl could be accomplished until it had been counteracted by the expansion waves from the shoulder.

The isentropic ramps were all reverse Prandtl-Meyer streamlines, the characteristics of which focused at a point on the initial oblique shock. The first of the isentropic inlets compressed the external flow down to Mach number 2.10 and the internal flow to nearly the minimum Mach number for starting. A modification of this inlet included a new cowl lip aligned in the local stream direction, together with an attendant elimination of most of the internal contraction. The second of these isentropic inlets compressed the external flow down to Mach number 1.88 and the internal flow to a near-maximum internal compression. The third inlet was designed to produce an all-external compression of the flow down to a Mach number of 1.55. The theoretical flow patterns of the single-wedge, double-wedge, and 1.88-isentropic inlets are presented in figures 2(a), (b), and (c), respectively.

Subsonic diffusers. - The variations in subsonic diffuser design are depicted in figures 1(c) and 3. The angle of divergence of one type, referred to as the short faired diffuser, had an over-all average value

of  $10^\circ$  and did not exceed  $12^\circ$  at any station (see fig. 1(c)). The average divergence angle of the short faired diffuser is then in accord with the optimum two-diverging-wall configuration indicated by Patterson (ref. 2). Another subsonic diffuser was designed to produce a theoretical pressure gradient proportional to the local static pressure (ref. 3). The resulting contour is shown in figure 1(c) and will be herein referred to as the trumpet diffuser. A long faired diffuser was also investigated (fig. 1(c)). This diffuser had an effective divergence angle of  $4^\circ$  to  $6^\circ$ , depending upon the compression wedge height, and this angle did not exceed  $7^\circ$  at any station.

Another subsonic diffuser was designed with an exit Mach number of 0.5 instead of the 0.2 value used in the previously mentioned diffusers. It is referred to as the high-velocity diffuser (fig. 1(c)). Another version of this high-velocity diffuser utilized extensive corner fillets on the long faired diffuser. Because this configuration resulted in a nearly oval exit cross section following the rectangular throat, it is referred to as the oval diffuser (fig. 3).

Internal area variations are presented in figure 4 for the double-wedge and 1.88-isentropic inlets. In general, the variations with type of subsonic diffuser are typical and change with compression surface only insofar as there is a slight variation in throat duct height. The long faired subsonic diffuser was modified by the addition of a variable second throat or constrictor located near the beginning of the diffuser. The position of this constrictor is indicated in figure 4(b) on the area-variation plot of the long faired diffuser. With this diffuser, the mass flow could be controlled by the use of the second throat, which could reduce the flow area by a factor of  $1/2$ . A final diffuser, referred to as the step diffuser, was also tested. This diffuser had a large area discontinuity at station 10.85 (3 in. downstream of the cowl lip), which is indicated in figure 4. (All stations are given in inches.)

For convenient reference, the designations and descriptions of all the subsonic diffuser configurations are summarized in table I.

Side plates. - Three side-plate configurations were investigated. The side plates, which were adjacent to the external compression surface were (1) rectangular side plates (fig. 1(a)); (2) swept side plates, the leading edges of which were swept back at the oblique-shock angle (fig. 1(b)); and (3) short side plates, the leading edges of which were located at the cowl-lip station. With the swept side plates it was necessary to employ very thin, sharp leading edges, approximately  $5^\circ$  with the free-stream direction, in order to stay below the shock-detachment value corresponding to the normal flow component.

### Instrumentation

The instrumentation (see figs. 1(b) and (c)) consisted of three ten-tube total-pressure rakes located on one side of the diffuser-exit chamber at station 26.5 or 37.5, depending on whether short or long diffusers were tested. Only the short faired, high-velocity, and trumpet diffusers used rakes located at station 26.5; all the other total-pressure data were taken at station 37.5. In order to establish the lateral symmetry of the flow, three total-pressure tubes were also installed on the opposite side of the chamber. In addition to the total-pressure tubes, one static-pressure tube and four wall static-pressure orifices were located at this station. In the diffuser-exit chamber (station 48) four wall static orifices were installed. In order to obtain a further indication of internal flow phenomena, a longitudinal row of wall static-pressure orifices was installed from the nose of the model to the end of the subsonic diffuser.

All pressure recoveries are presented as ratios of the total pressure at the diffuser exit to free-stream total pressure ( $P/P_0$ ). The mass flows are also presented in the form of a ratio, a measured mass flow to a calculated supercritical mass flow with no spillage ( $m/m_0$ ). The range of stability is indicated by the ratio of the measured supercritical minus the lowest stable subcritical mass flow divided by the calculated supercritical mass flow with no spillage ( $\Delta m/m_0$ ).

The average total-pressure recovery and capture mass flow were based on the area ratios at the model exit, the measured static pressures at station 48, and the sonic discharge area. The resulting values were approximately the same as those obtained by an area integration of the rake pressures. The rake data were used to determine the total-pressure profiles. In addition, a correction factor was applied so that the single-wedge inlet with swept side plates would have a supercritical mass-flow ratio of unity. This procedure was permissible since the oblique shock appeared to intersect the cowl lip. The correction factor was found to be a function of Reynolds number. This correction (1.04 times experimental mass flow at a Reynolds number of  $0.5 \times 10^6$ ) was applied to each inlet.

A spark twin-mirror schlieren system and high-speed movie camera arrangement were used to observe the inlet air-flow patterns.

### RESULTS

The effects on pressure recovery, mass flow, and stability range of compression surface, subsonic diffuser, and side-plate configuration are summarized in tables II, III, and IV, respectively. These results, together with visual flow observations, are discussed in the following section.

No effect of Reynolds number on pressure recovery or mass flow was observed for the range investigated. There was, however, an effect of Reynolds number and initial surface roughness on stability range. This subcritical-operation effect is discussed separately in a later section. In no case did the addition of leading-edge roughness improve the performance.

#### Effects of Compression Surface on Performance

Pressure recovery and mass-flow characteristics. - As indicated in table II and figure 5, pressure recovery generally increased in the following order for the supersonic compression surfaces investigated: single wedge, 2.10 isentropic, double wedge, 1.55 isentropic, and 1.88 isentropic. This trend was observed for both the critical and the maximum recovery conditions. This sequence was theoretically anticipated, except for the 1.55-isentropic inlet, which employed the greatest amount of compressive flow turning. With this inlet, it was observed that a bow shock stood ahead of the cowl lip considerably farther than with the 1.88-isentropic inlet, even though the mass-flow ratios were not much different. This bow shock resulted from turning in excess of the theoretical compression limit indicated in reference 4.

The optimum recovery of 0.71 was obtained with the 1.88-isentropic inlet with the oval subsonic diffuser and rectangular side plates. The corresponding mass-flow ratio was 0.965. The respective critical pressure recovery and mass flow for the remaining inlets were as follows: single-wedge inlet with a short faired diffuser, 0.41 and 1.0; double-wedge inlet with a long faired diffuser, 0.605 and 0.99; 2.10-isentropic inlet with long faired diffuser, 0.58 and 0.93; and 1.55-isentropic inlet with long faired diffuser, 0.65 and 0.94. All these inlets utilized swept side plates.

Typical diffuser-exit profiles obtained with the 1.88-isentropic inlet are presented in figure 5. In general, there were some indications of separated flow in each case; however, the long subsonic diffuser configurations exhibited less-severe distortions in exit total-pressure profile. Indications of the thick boundary layer on the compression surfaces (with and without an inlet cowl) may be seen in the schlieren photographs of figure 6.

Inlet stability characteristics. - Some degree of stable subcritical operation was realized with each configuration. Some of this operation at reduced mass-flow, however, was coincident with a slight local oscillation of the diffuser shock. Under these conditions the instantaneous pressure variations at the diffuser exit were believed to be negligibly small (certainly in relation to inlet buzz) and the operation of the inlet was considered essentially stable. There was no discernible trend in the size of the subcritical stable range with the type of supersonic compression surface employed.

3730 Motion-picture studies (approximately 600 frames/sec) were taken during buzz operation of the 2.10-isentropic inlet utilizing a long faired subsonic diffuser and long glass side plates. A selected sequence of pictures is shown in figure 7 to illustrate typical flow patterns observed during a pulse cycle. In its most downstream position (zero time) the diffuser shock was located well back in the subsonic diffuser. As the shock moved forward toward the throat, extensive separation was observed immediately downstream thereof (0.030 sec). With the diffuser shock passing through the throat, the boundary layer on the wedge shoulder lifted off the surface (0.033 sec) and thereby tended to choke off the inlet flow (0.037 sec). Separation then moved upstream along the contoured compression surface and finally extended all the way to the leading edge, with correspondingly large amounts of flow spillage (0.042 sec). The frequency of pulsing in this case was approximately 17 cycles per second. There appeared to be an interaction between the tunnel and inlet flows, however, when the bow shock was in its most upstream position. The resulting coupling may have had some influence on the buzz phenomenon with regard to frequency and amplitude. The time interval between the first disturbance of the lip shock and complete disruption of the flow is of the order of 0.008 to 0.017 second for the 2.10-isentropic inlet. This interval was roughly checked (0.008 sec) by a calculated time for a plane sound wave to travel from inlet to exit and back.

As noted previously, small regions of low-amplitude shock oscillation were detected during subcritical operation. In such conditions, it is believed that the resulting pressure oscillations are reasonably small and that the inlet operation can be considered essentially stable. Although no definite trend from one inlet to another has been observed, an effect of Reynolds number upon this local shock unsteadiness was noted for some of the inlets. The origin of these oscillations may lie in pressure feedback through localized separated areas produced by boundary-layer-shock interactions on the ramp or by the flow around the sharp-lip cowl. In contrast to these local oscillations, both the critical point and the onset of full inlet buzz were generally insensitive to Reynolds number.

Occasionally during supercritical inlet operation and for a small range of exit-plug positions, there were observed large-amplitude pressure oscillations which were attributed to an erratic positioning of the normal shock. With the aid of the glass side plates this phenomenon was observed to occur when the normal shock in the subsonic diffuser was located at a position where an internal shock reflected from the diffuser wall.

Visual flow observations. - In figure 8 some observations of subcritical flow patterns are presented. Two distinct types of subcritical flow structure were encountered. The first was obtained with the single-wedge (wedge-surface Mach number equal to 2.08) and the 2.10-isentropic inlets (figs. 8(a), (b), and (d)). In these cases, extensive separation off the wedge surfaces was observed with the vortex sheet from the

strong shock intersection appearing to be nearly straight and inclined at an angle indicating flow deflection away from the wedge. The second type of subcritical flow structure was observed with the double-wedge (wedge-surface Mach number equal to 1.91), 1.88-isentropic, and 1.55-isentropic inlets (figs. 8(c) and (e)). This pattern indicated little or no flow separation on the wedge surface. The vortex sheet from the shock intersection has a pronounced curvature, which, contrary to the first type, shows an initial flow deflection towards the compression surface. This curvature supports the observation that the inlet flow behind the diffuser normal shock reaccelerates to sonic and then supersonic velocities with additional shocks occurring at the diffuser entrance. In addition, stable subcritical shock configurations of the second type were much steadier than those of the first type. This difference in type of flow pattern may be related to some local Mach number effect, since the first type occurred only on inlets where the local Mach number was 2.08 or above. Conversely, it was observed that a steady bow shock with a flow structure of the second type never was located on a compression surface where the local Mach number was greater than 1.91.

The separation angle observed during subcritical operation of the single-wedge inlet was constant at approximately  $9^\circ$  (within the accuracy of measured separation shock angles) as the point of separation (and thus local Reynolds number) varied along the wedge surface (figs. 8(a) and (b)). Forward-facing-step data would indicate a separation angle of  $10.5^\circ$ .

With supercritical inlet operation, local areas of flow separation were observed in some cases just downstream of the wedge shoulder. This separation was most prominent with the single-wedge configuration (fig. 9) and was the result of the cowl-lip shock impinging downstream of the shoulder. The attendant flow pattern was typical of extensive shock-boundary-layer interactions where the flow reattaches to the wall at some downstream position. An analysis, using the separation criteria of Lange (ref. 5) for forward-facing wedges and Chapman's criteria (ref. 6) for rearward-facing steps, was made in an attempt to predict this separation pattern. The results are illustrated in figure 10 for the single-wedge inlet. A trial-and-error procedure was employed to determine the location of point i (point of separation) on the favorable-pressure-gradient turn of the wedge shoulder. The angle of separation was determined from reference 5 and the reattachment angle from reference 6. The method of reference 6 requires that the downstream flow reattach to the wall (point ii) at the local oblique-shock detachment angle. Qualitatively, at least, the method predicted this particular flow field.

As demonstrated in reference 7, this local separation can be minimized or eliminated through the use of wall suction or by redesigning the cowl lip to have the point of shock impingement located on the favorable-pressure-gradient turn. Observations of the flow near the throats of the double-wedge and isentropic inlets (figs. 6(b) and (c))

accordingly showed little local separation after the turn, since in these instances the cowl-lip shocks appeared to impinge close to or on the favorable-pressure-gradient region.

Since local separation near the throat and an accompanying bow shock were observed during supercritical operation for the 1.55-isentropic inlet with a long faired diffuser and rectangular side plates, wall suction was applied through a slot located immediately downstream of the shoulder. Suction was obtained by venting to free-stream static pressure. Without suction there was some local separation after the turn and supercritically a detached bow shock stood ahead of the cowl lip. As indicated in figure 11(a), a hysteresis loop was encountered in the diffuser performance curve. For comparison, the inlet performance with the use of suction and the short-side-plate modification is presented. The total-pressure profiles for the suction case are also presented (fig. 11(b)). The schlieren observations which correspond to flow conditions on either side of this discontinuity (that is, the vertical branches on the hysteresis loop) are shown by the photographs of figures 12(a) and (b). The minimum stable subcritical flow is shown in figure 12(c). With the application of suction (fig. 12(d)), the flow at the cowl lip appeared to be attached with the compression waves coalescing at the lip. In this case, no local separation was observed near the throat. With suction, gains in pressure recovery, supercritical mass flow, and stability range were realized when compared with the corresponding no-suction configuration.

Another example of localized separation is shown in figure 13 and in the schematic sketches of these photographs. In this case, the internal contour of the cowl had a high rate of turning from the initial angle back toward the axial direction. The amount of compressive turning along the cowl exceeded the Prandtl angle corresponding to the initial Mach number before it attained the cancellation benefits of expansion waves from the wedge shoulder. This configuration was the 1.88-isentropic inlet utilizing the trumpet diffuser and rectangular side plates with a special cowl. As illustrated in figure 13(a), the flow separated locally along the internal contour in a chordwise manner across the high curvature portion of the cowl. As the back pressure was increased, the point of separation gradually moved upstream to the leading edge of the cowl, at which time a disturbance to the lip shock system occurred. Thus, critical flow was obtained with the terminal shock well inside the inlet. Photographs of supercritical and slightly subcritical flows, which exemplify this separation on the cowl surface, are presented in figure 13. At critical pressure recovery the location of separation becomes erratic as indicated in the sketch. This phenomenon was also noticed in inlets where there existed a system of strong shocks in the throat, due perhaps to a localized choking condition caused by severe separations on the wedge side of the passage.

Another method by which premature subcritical inlet operation occurred was by means of a subsonic layer along the internal contour of

the lip. This method again furnished a path for feedback of pressure disturbances originating from an unsteady terminal shock located in the diffuser. This condition arose when the cowl of the 1.88-isentropic inlet was located above the point of shock coalescence. This type of flow was also noticed with the double-wedge inlet. In each case, shock detachment resulted in a subsonic layer of air flow between the cowl surface and the vortex sheet from the shock intersection. This condition was eliminated on the double-wedge inlet by a repositioning of the cowl.

### Effects of Subsonic Diffuser on Performance

Pressure recovery and mass-flow characteristics. - The effects that various subsonic diffusers have upon the performance of the various inlets may be determined from the data in table III. Because the performance of the short faired diffuser is nearly the same as that of the trumpet diffuser, no distinction between the two is made in table III. Typical curves of total-pressure recovery against mass-flow ratio are presented in figures 14(a) and (b). With subsonic diffusers as the only variable, the critical and maximum pressure recoveries consistently increased in the following order: short faired, long faired, high-velocity, and oval diffusers. A short subsonic diffuser generally resulted in a badly separated profile at the diffuser exit with an accompanying loss in pressure recovery of approximately 0.05 when compared with that of the long faired diffusers. The long faired diffuser also resulted in a decrease in exit-profile distortion from that obtained with the short faired subsonic diffuser. Typical exit profiles are also presented for the oval subsonic diffuser with rectangular side plates in figure 14(c) and for the high-velocity diffuser with swept side plates in figure 14(d).

The high-velocity diffuser with rectangular cross section yielded a high pressure recovery (0.70) but had an accompanying large profile distortion (see fig. 14). For this subsonic diffuser, the rate of divergence is even more gradual than that of the long faired diffuser. A similar high-exit-Mach-number diffuser, but with oval cross section (oval diffuser), gave the performance indicated in figure 14. Only a very slight increase in recovery (0.715) was realized over that for the high-velocity diffuser with rectangular cross section. The contour plot of figure 14 illustrates the boundary-layer accumulation at the centerline on the ramp side of the duct due to the pressure gradient arising from a centrifugal effect on the main flow. In general, this observation is true of all the duct designs studied herein. A modified long faired diffuser with 3.5 hydraulic diameters of zero diffusion length (as used in ref. 8 for flow stabilization) gave results essentially the same as those for the original long faired diffuser. The use of gradual rates of area divergence and long ( $4^\circ$  included angle) subsonic diffusers was necessary for high performance. The use of long diffusers, of course, may not be the most desirable solution, since it adds length and weight to the aircraft.

In order to investigate further the effectiveness of the subsonic diffusers, wall-static pressures were obtained from the leading edge of the wedge to the end of the diffuser section for both the short and the long diffusers. These data for the double-wedge inlet are presented in figure 15. Wall pressure distributions are given for several operating conditions; that is, subcritical, critical, and supercritical for both diffusers. The trends of static pressures up to the minimum-area section are as might be expected, but because of the extensive flow separation and the complex diffuser shock system in supercritical operation, no single normal shock is indicated by the pressure data. There is an improvement in diffusion (i.e., an increase in static-pressure rise and thus a decrease in exit Mach number) by using the long faired subsonic diffuser, especially during operation at critical or supercritical conditions.

Inlet stability. - As indicated in figure 14, the largest stable subcritical operating range was realized with the 1.88-isentropic inlet utilizing the oval diffuser and both the short and the rectangular side plates. These configurations were stable for ranges of mass-flow ratio down to 0.60, whereas the swept-side-plate configuration decreased the stability to a mass-flow ratio of 0.81. The subcritical stability ranges of the short- and rectangular-side-plate configurations were extended beyond that obtained with the short subsonic diffusers. The oval subsonic diffuser has an extremely gradual area divergence (see fig. 4) and its cross-sectional area undergoes a transition from a rectangular throat to an oval-shaped exit. At the critical operating condition, this inlet demonstrated relatively high performance (pressure recovery of 0.71 and mass-flow ratio of 0.965).

The performance of the step subsonic diffuser as shown in figure 14(a) is of interest on the basis of stability. Initially, the configuration was tested to determine its pressure-recovery performance (theoretical peak recovery equaled 0.66 with the assumption of complete loss of dynamic pressure behind the normal shock) and to compare its results with the inlets having the shorter subsonic diffusers. Boundary-layer thickening at the throat, due to pressure feedback, resulted in a pressure recovery of only 0.52. However, the subcritical stability range was extended beyond that obtained with the trumpet or short faired subsonic diffusers.

Schlieren photographs are presented in figure 16(a) for critical and stable subcritical operating conditions. For subcritical operating conditions, the diffuser bow shock stands stably out on the isentropic compression surface. The local-flow Mach number just ahead of this strong shock is of the order of 1.9, which is considerably greater than the suggested value of 1.33 necessary for separation of a turbulent layer by means of a normal shock (ref. 9). In this case, while separation may

3730

CB-2 back

occur locally at the point of shock-boundary-layer interaction, the flow downstream of this zone does not seem to be separated; however, the apparent boundary layer after interaction is markedly thicker. As indicated by the high curvature of the vortex sheet just downstream of the main intersection and the secondary shocks at the diffuser entrance, the flow behind the diffuser normal shock appears to reaccelerate to sonic and then to supersonic velocities with additional shocks at the entrance. The favorable pressure gradient of this reacceleration may assist in the reattachment of the boundary layer.

Another configuration of interest on the basis of stability is the 1.88-isentropic inlet with a long faired subsonic diffuser and a variable second throat, which could vary the geometric flow area near the beginning of the subsonic diffuser. The diffuser performance characteristics are presented in figure 14. The stable subcritical range was effectively extended by means of the variable-area throat device. A sequence of schlieren photographs in figure 16(b) illustrates the flow mechanisms involved. The exit plug is at a fixed setting and the second throat is progressively closed. Initially the flow across the constrictor is supersonic. When the second throat is closed, the flow in the throat is choked and a strong shock system is formed upstream which progressively moves out ahead of the diffuser entrance to the minimum stable mass-flow position, as indicated in the lower photograph. At the same time, a strong shock structure exists downstream of the throat and appears to remain in a fixed location. The solid circles (fig. 14(b)) represent conditions with the second throat fixed in an open position and the exit plug varying over a wide range of axial positions. The open circles indicate operation of the second throat at several fixed settings of the exit plug. As shown, this device adds some flexibility to the operation of the inlet in that stable flow at reduced mass flows can be obtained over a wide range of pressure levels. Presumably, regulation of mass flow by means of the second throat yields a greater stable range, because the resonant volume or length of the diffuser is reduced. With the choking position so near the inlet, the time lag between a movement of the shock and the accommodation reaction at the throat is so small that large-amplitude mass-flow oscillations are avoided, and there is a reduced tendency of the inlet towards resonant pulsing.

Visual flow observations. - With the inlet well supercritical, the short subsonic diffuser configurations incurred extensive separation of the boundary layer off the contoured surface where the wall angles started to increase rapidly (for example, the short diffuser in fig. 9). With the longer diffusers, the field of view did not extend the entire length, and with the diffuser flow supersonic, no evidence of separation was noted. As the diffuser terminal-shock system moved upstream with increased back pressure, separation in all cases was observed immediately

3730 downstream thereof and appeared more pronounced with the shorter diffusers. The diffuser-shock structure, consisting of a multiple-shock system inside the duct (fig. 6), formed into a single shock structure when positioned near the throat or forward of the cowl lip. Critical inlet operation was generally achieved with the diffuser-shock system located some distance downstream of the throat. Upstream movement of this shock was accompanied by a lifting or separating of the boundary layer forward to the wedge shoulder (see figs. 9(b) and (c)) and by some adjustment of the shocks at the cowl lip with attendant flow spillage. This effect may be attributed to a pressure feedback through the boundary layer or local areas of separation along the wedge surfaces. A time variation of the throat flow area is experienced when the boundary layer is separated. Consequently, this may result in a variation in spilled mass flow and thus an unsteadiness in the bow shock.

#### Effects of Side Plate on Performance

Pressure recovery and mass-flow characteristics. - As shown in table IV and figure 17, the supercritical mass flow and critical pressure recovery for the short-side-plate installation was generally less than that for the respective inlet with rectangular or swept side plates. The maximum pressure recovery for the swept inlet configuration was generally equal to or greater than that for inlets which incorporated rectangular side plates.

Inlet stability. - Generally, the short-side-plate configuration gave better stability characteristics than the rectangular- or swept-side-plate configurations.

The range of improvement varied from an actual loss in the single-wedge inlet to a gain ( $\Delta m/m_0 = 0.13$ ) with the double-wedge inlet utilizing a short diffuser.

Visual flow observations. - With the glass side plates, a pronounced interaction was observed between the inlet-shock system and the side-plate boundary layer (see fig. 9). Evidences of this interaction are identified by the lines labeled b and a in figure 9(b). Disturbance b is probably due to the thickening or separation of the boundary layer from the side plates, since it lies just behind the initial shock and is not as noticeable with the double-wedge and isentropic inlets, which have weaker oblique shocks. The consequence of this effect is a thickened (if not locally separated) boundary layer with some associated spillage of the flow out of the inlet near the outer edges of the cowl lip. This result, of course, is avoided by the use of swept side plates. This thickened boundary layer experiences an adverse pressure gradient as it is turned in the axial direction by the lip. This additional adverse effect separates the boundary layer and generates the small corner shocks, designated by a in figure 9(b).

## DISCUSSION

The range of inlet design was selected to determine if the potentially higher compression inlets (such as the isentropic), in the final comparison, would yield a sufficiently better performance to outweigh the simplicity and lower drag potential of the single-wedge configuration. Generally, the performance levels of the two-dimensional inlets were somewhat below those obtained with comparable axisymmetric models. This lower performance might have been expected, since the two-dimensional inlets were likely to have had adverse performance effects because of square corners and thicker compression surface boundary layers. At Mach number 3.05 the optimum internal-flow performance was obtained with the 1.88-isentropic inlet utilizing the oval diffuser and rectangular side plates. A critical total-pressure recovery of 0.71 was realized with a corresponding mass-flow ratio of 0.965. These values compare with a recovery of 0.77 and mass-flow ratio of 0.92 obtained in reference 10 with an axisymmetric isentropic inlet. This particular axisymmetric inlet, however, carried the external compression down to a Mach number of 1.76 instead of the 1.88 used in the present two-dimensional case (both inlets incorporated internal compression). Thus, there is a possibility of further improvement of the two-dimensional inlet.

The largest detrimental effect on the pressure recoveries and profiles was the separation of the boundary layer downstream of the terminal shock on the ramp side of the inlet. Although this separation was minimized to some extent by the use of long faired diffusers, no means was found to eliminate it completely. In every case, the boundary layer on the compression surface was a sizeable portion of the entering air flow. The interaction of this boundary layer with the terminal-shock system in the subsonic diffuser resulted in extensive separation of the flow from the wall. This flow did not reattach. Although the boundary-layer height seemed to be decreased by the action of the favorable pressure gradient on the wedge shoulder (1.88-isentropic wedge and no cowl), it immediately thickened upon interaction with the strong shock system.

Figure 18 summarizes the maximum performance of the various inlets (including the axisymmetric inlet of ref. 10) and indicates what combination of the geometric variables was necessary in order to obtain the performance. Both the critical and peak pressure recoveries are indicated with the respective mass-flow ratios. In addition, the theoretical recoveries of the various inlets, neglecting subsonic losses, are also presented. Some approximate calculations showed that the relative performance based on a thrust-minus-drag consideration would be the same as that indicated solely by the pressure data. Cowl-pressure and supercritical additive drags were the only drags considered in these calculations, which scaled the inlets so that each captured the same mass flow. With these drags estimated by two-dimensional shock-expansion

theory and with assumed values of total-pressure ratio and total-temperature ratio across a hypothetical ram jet, thrust-minus-drag values could readily be obtained from the charts of reference 11.

### SUMMARY OF RESULTS

The results of the experimental investigation to evaluate the performance capabilities of two-dimensional inlets at a Mach number of approximately 3.1 are as follows:

1. The performance levels of the two-dimensional inlets were somewhat below those obtained previously with comparable axisymmetric models.

2. The optimum performance was obtained with the 1.88-isentropic inlet utilizing a subsonic diffuser with oval cross section and rectangular side plates. A critical total-pressure recovery of 0.71 was realized with a corresponding mass-flow ratio of 0.965. Subcritical stability to a mass-flow ratio of 0.60 was obtained.

3. The respective critical pressure recovery and mass flow for the remaining inlets were as follows: single-wedge inlet with a short faired diffuser, 0.41 and 1.0; double-wedge inlet with a long faired diffuser, 0.605 and 0.99; 2.10-isentropic inlet with long faired diffuser, 0.58 and 0.93; and 1.55-isentropic inlet with long faired diffuser, 0.65 and 0.94. All these inlets utilized swept side plates.

4. Long faired subsonic diffusers (over-all angle of divergence  $\sim 4^\circ$ ) gave an increase in pressure recovery of approximately 0.05 over that for short diffusers (over-all angle of divergence  $\sim 10^\circ$ ).

5. For the range investigated, Reynolds number generally had little or no effect upon inlet performance. In no case did the addition of leading-edge roughness improve performance.

6. Although pressure recovery and mass flow were reduced with the use of short side plates, the range of stable subcritical operation was somewhat extended. Inlets that incorporated the oval diffuser, the step diffuser, and the throat constrictor gave improved inlet stability over that obtained with the short subsonic diffuser configurations.

7. As the diffuser terminal-shock system moved upstream with increased back pressure, separation in all cases was observed immediately downstream thereof and appeared more pronounced with the shorter diffusers.

8. As a result of pressure feedback through locally separated areas along the inside of the cowl, critical inlet operation occurred with the terminal shock located well downstream inside the diffuser.

Lewis Flight Propulsion Laboratory  
National Advisory Committee for Aeronautics  
Cleveland, Ohio, November 3, 1955

#### REFERENCES

1. Connors, James F., and Woollett, Richard R.: Experimental Investigation of a Two-Dimensional Split-Wing Ram-Jet Inlet at Mach Number of 3.85. NACA RM E52F04, 1952.
2. Patterson, G. N.: Modern Diffuser Design. Aircraft Eng., vol. X, no. 115, Sept. 1938, pp. 267-273.
3. Davis, Wallace F., Edwards, Sherman S., and Brajnikoff, George B.: Experimental Investigation at Supersonic Speeds of Twin-Scoop Duct Inlets of Equal Area. IV - Some Effects of Internal Duct Shape Upon an Inlet Enclosing 31.2 Percent of the Forebody Circumference. NACA RM A9A31, 1949.
4. Connors, James F., and Meyer, Rudolph C.: Design Criteria for Axisymmetric and Two-Dimensional Supersonic Inlets and Exits. NACA TN 3589, 1956.
5. Lange, Roy H.: Present Status of Information Relative to the Prediction of Shock-Induced Boundary-Layer Separation. NACA TN 3065, 1954.
6. Chapman, Dean R.: An Analysis of Base Pressure at Supersonic Velocities and Comparison with Experiment. NACA Rep. 1051, 1951. (Supersedes NACA TN 2137.)
7. Connors, James F., and Woollett, Richard R.: Some Observations of Flow at the Throat of a Two-Dimensional Diffuser at Mach Number of 3.85. NACA RM E52I04, 1952.
8. Nettles, J. C.: The Effect of Initial Rate of Subsonic Diffusion on the Stable Subcritical Mass-Flow Range of a Conical Shock Diffuser. NACA RM E53E26, 1953.
9. Nussdorfer, T. J.: Some Observations of Shock-Induced Turbulent Separation on Supersonic Diffusers. NACA RM E51L26, 1954.

10. Hunczak, Henry R.: Pressure Recovery and Mass-Flow Performance of Four Annular Nose Inlets Operating in Mach Number Region of 3.1 and Reynolds Number Range of Approximately  $0.45 \times 10^6$  to  $2.20 \times 10^6$ . NACA RM E54A07, 1954.
11. Kremzier, Emil J.: A Method for Evaluating the Effects of Drag and Inlet Pressure Recovery on Propulsion-System Performance. NACA TN 3261, 1954.

3730

CB-3

TABLE I. - SUBSONIC-DIFFUSER CONFIGURATIONS

Designation	Description
Trumpet diffuser	Trumpet shaped; local pressure gradient proportional to local static pressure; over-all angle of divergence equal to $10^\circ$
Short diffuser	Short arbitrary contour; over-all angle of divergence equal to $10^\circ$ ; maximum turning angle equal to $12^\circ$
Long faired diffuser	Long arbitrary contour; over-all angle of divergence equal to $4^\circ$ ; maximum turning angle equal to $6^\circ$
Oval diffuser	Long, high exit Mach number (design exit Mach number, 0.5); transition to oval cross-sectional areas
High-velocity diffuser	Short, high exit Mach number (design exit Mach number, 0.5); all rectangular cross-sectional areas
Second-throat diffuser	Same as long faired diffuser but with variable-throat constrictor
Step diffuser	Abrupt area discontinuity at throat, thus causing flow to be penalized by loss of dynamic pressure

TABLE II. - EFFECT OF COMPRESSION SURFACE ON PERFORMANCE

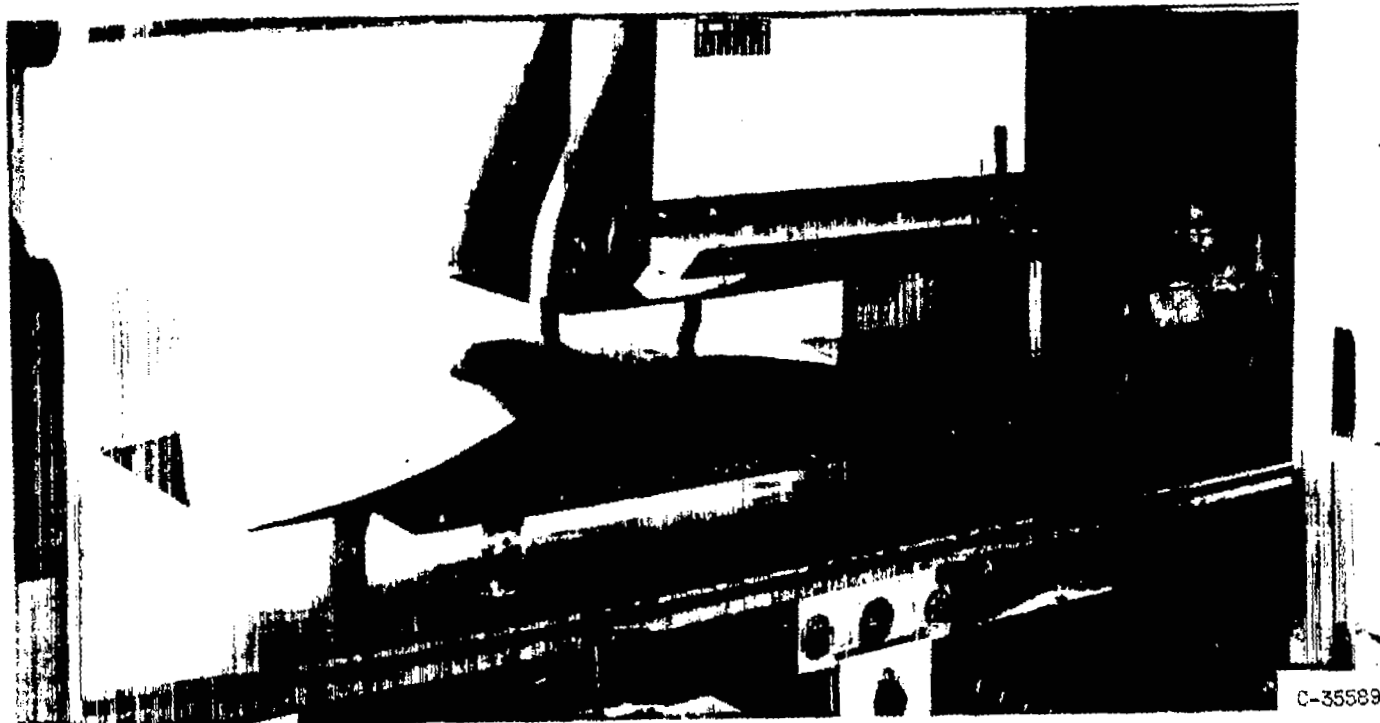
Compression surface	Subsonic diffuser	Side plate	Pressure recovery, $P/P_0$		Supercritical mass flow, $m/m_0$	Range of stability, $\Delta m/m_0$
			Critical	Maximum		
Single wedge	Short	Rectangular	0.39	0.41	0.95	0.15
Double wedge	Short	Rectangular	.48	.53	.92	.21
2.10 Isentropic	Short	Rectangular	.50	.53	.92	.07
1.88 Isentropic	Short	Rectangular	.61	.625	.925	.09
Single wedge	Short	Swept	.41	.41	1.0	.24
Double wedge	Short	Swept	.46	.535	.94	.11
1.88 Isentropic	Short	Swept	.64	.65	.925	.11
Single wedge	Short	Short	.40	.40	.93	.19
Double wedge	Short	Short	.44	.55	.91	.24
1.88 Isentropic	Short	Short	.585	.61	.875	.14
Double wedge	Long	Rectangular	.585	.60	.99	.15
2.10 Isentropic	Long	Rectangular	.565	.57	.93	.07
1.88 Isentropic	Long	Rectangular	.675	.68	.93	.11
1.55 Isentropic	Long	Rectangular	.62	.625	.92	.21
1.55 Isentropic	Long suction	Rectangular	.625	.67	.94	.295
Double wedge	Long	Swept	.605	.62	.99	.12
2.10 Isentropic	Long	Swept	.58	.58	.93	.095
1.88 Isentropic	Long	Swept	.665	.69	.95	.12
1.55 Isentropic	Long	Swept	.65	.69	.94	.165
2.10 Isentropic	Long	Short	.53	.55	.875	.12
1.55 Isentropic	Long	Short	.615	.63	.85	.26
1.88 Isentropic	Oval	Rectangular	.71	.71	.965	.365

TABLE III. - EFFECT OF SUBSONIC DIFFUSER ON PERFORMANCE

Compression surface	Subsonic diffuser	Side plate	Pressure recovery, $P/P_0$		Supercritical mass flow, $m/m_0$	Range of stability, $\Delta m/m_0$
			Critical	Maximum		
Double wedge	Short	Swept	0.46	0.535	0.94	0.11
Double wedge	Long	Swept	.605	.62	.99	.12
2.10 Isentropic	Short	Rectangular	.50	.53	.92	.07
2.10 Isentropic	Long	Rectangular	.565	.57	.93	.07
1.88 Isentropic	Short	Rectangular	.615	.625	.925	.095
1.88 Isentropic	Long	Rectangular	.675	.68	.93	.12
1.88 Isentropic	High velocity	Rectangular	.68	.705	.97	.095
1.88 Isentropic	Oval	Rectangular	.71	.71	.965	.365
1.88 Isentropic	Step	Rectangular	.485	.53	.945	.265
1.88 Isentropic	Constrictor	Rectangular	.665	.68	.97	.23
1.88 Isentropic	Short	Swept	.64	.65	.925	.11
1.88 Isentropic	Long	Swept	.665	.69	.95	.12
1.88 Isentropic	High velocity	Swept	.69	.70	.955	.155
1.88 Isentropic	Oval	Swept	.70	.715	.95	.14
1.88 Isentropic	Short	Short	.585	.61	.875	.14
1.88 Isentropic	High velocity	Short	.65	.66	.91	.155
1.88 Isentropic	Oval	Short	.695	.695	.90	.435

TABLE IV. - EFFECT OF SIDE PLATE ON PERFORMANCE

Compression surface	Subsonic diffuser	Side plate	Pressure recovery, $P/P_0$		Supercritical mass flow, $m/m_0$	Range of stability, $\Delta m/m_0$
			Critical	Maximum		
Single wedge	Short	Swept	0.41	0.41	1.0	0.24
Single wedge	Short	Rectangular	.39	.41	.95	.15
Single wedge	Short	Short	.40	.40	.93	.19
Double wedge	Short	Swept	.46	.535	.94	.11
Double wedge	Short	Rectangular	.48	.53	.92	.21
Double wedge	Short	Short	.44	.55	.91	.24
1.88 Isentropic	Short	Swept	.64	.65	.925	.11
1.88 Isentropic	Short	Rectangular	.61	.625	.925	.095
1.88 Isentropic	Short	Short	.585	.61	.91	.15
Double wedge	Long	Swept	.605	.62	.99	.12
Double wedge	Long	Rectangular	.585	.60	.99	.15
2.10 Isentropic	Long	Swept	.58	.58	.93	.095
2.10 Isentropic	Long	Rectangular	.565	.57	.97	.07
2.10 Isentropic	Long	Short	.53	.55	.875	.12
1.88 Isentropic	Long	Swept	.665	.69	.95	.12
1.88 Isentropic	Long	Rectangular	.675	.68	.93	.11
1.88 Isentropic	High velocity	Swept	.69	.70	.955	.155
1.88 Isentropic	High velocity	Rectangular	.68	.705	.97	.095
1.88 Isentropic	High velocity	Short	.65	.66	.91	.155



(a) Model installation in Mach number 3.12 tunnel.



(b) Fake instrumentation and movable exit plug of model.

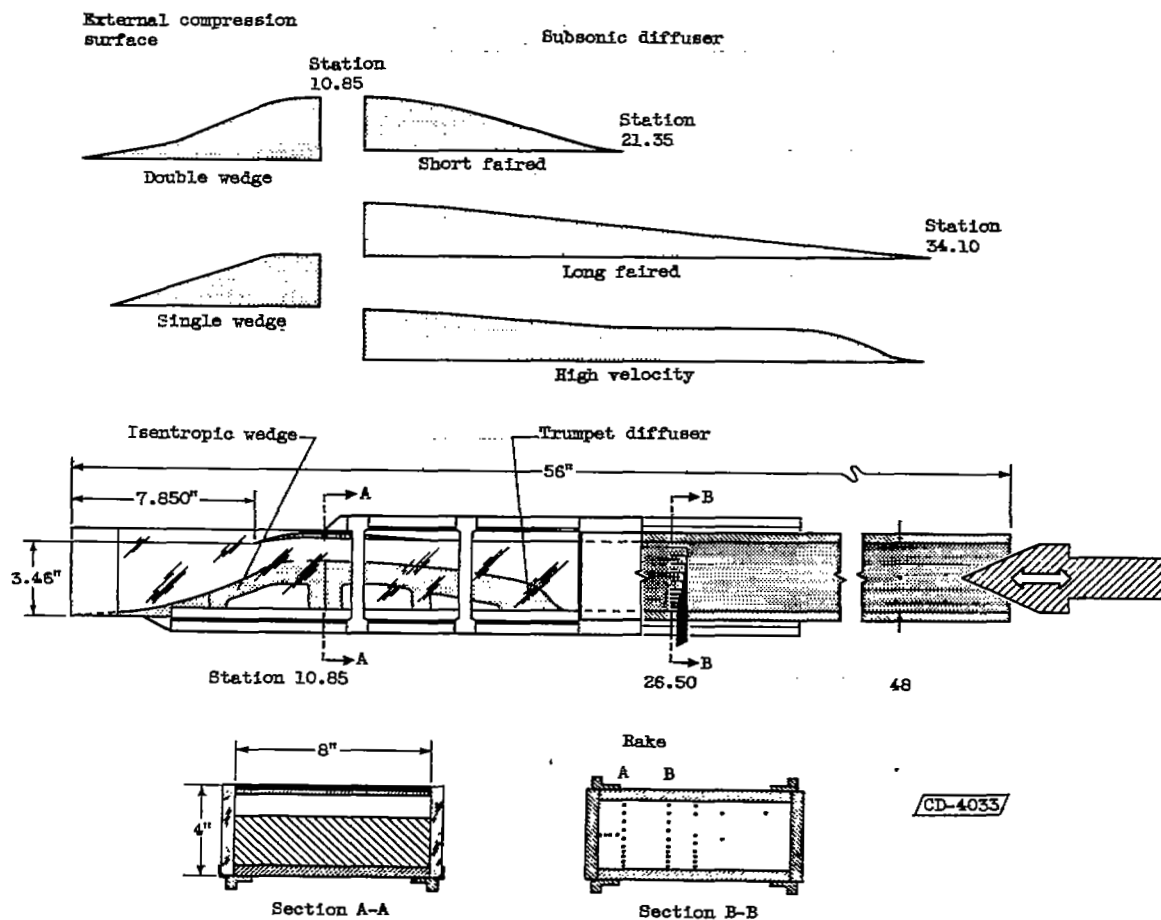
Figure 1. - Two-dimensional inlet model.

33

NACA RM E55K01

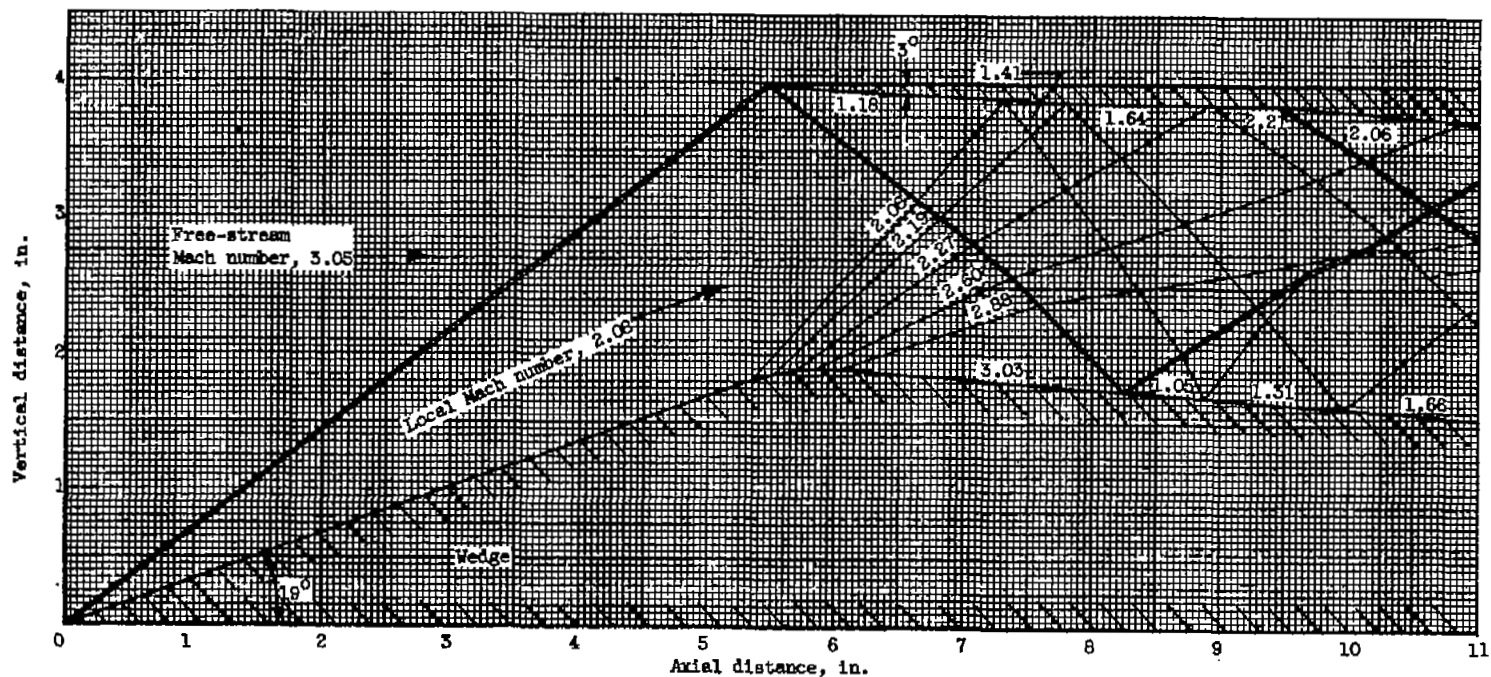
C-35706

3730



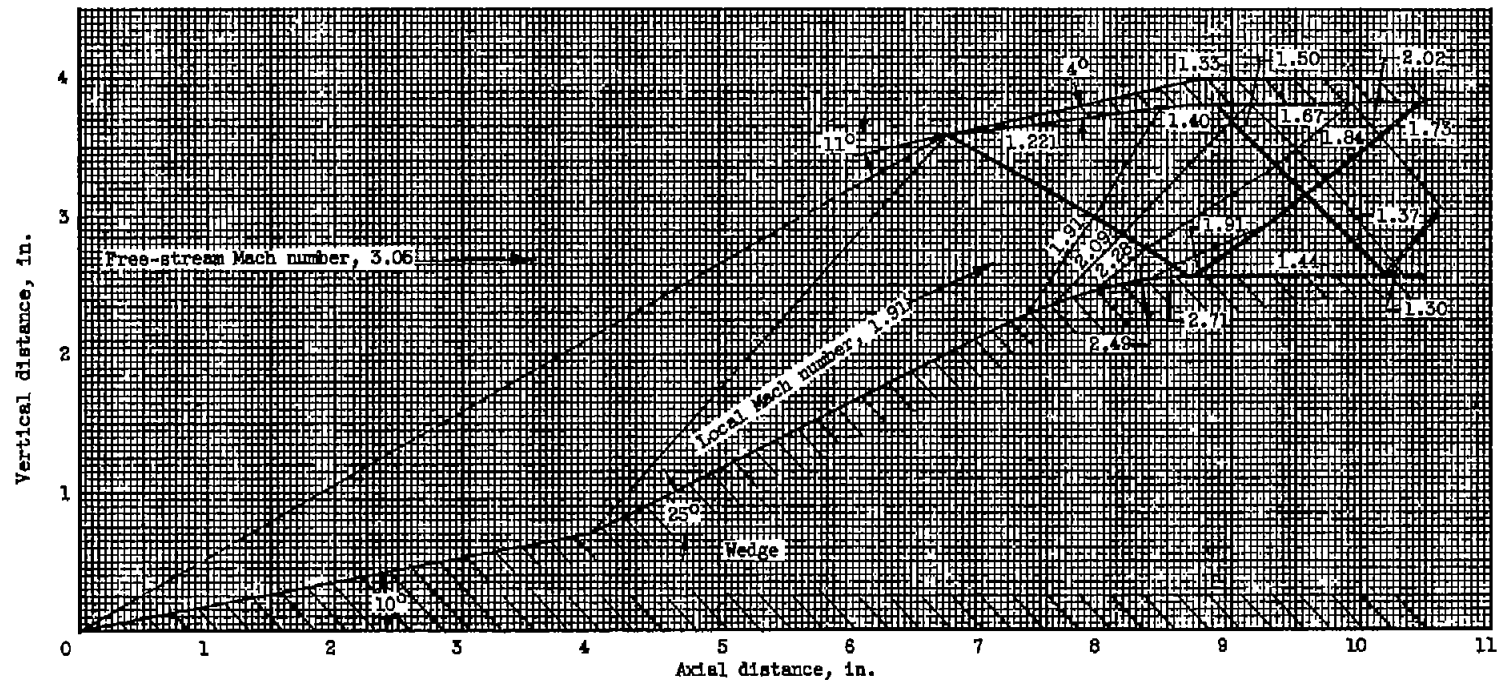
(c) Various components of model. (Stations measured in inches from leading edge of rectangular side plates.)

Figure 1. - Concluded. Two-dimensional inlet model.



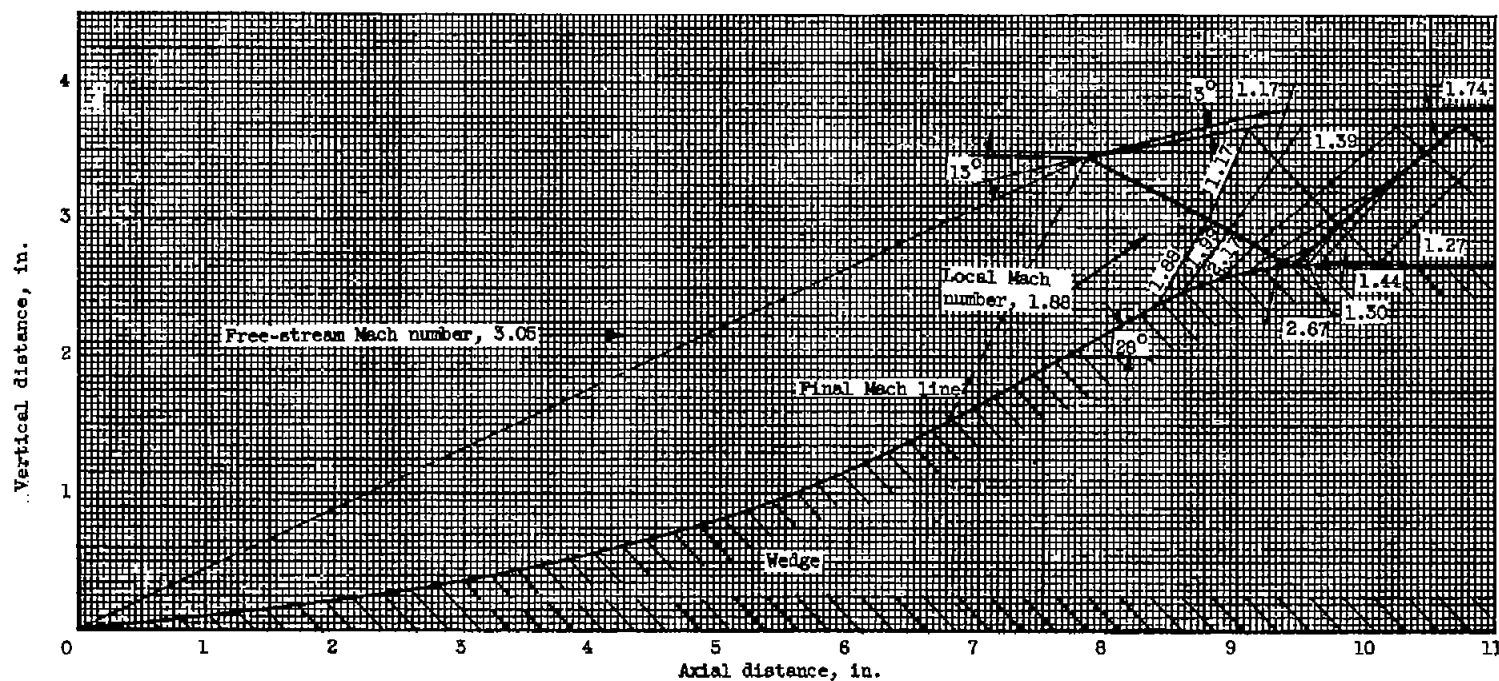
(a) Single-wedge inlet.

Figure 2. - Theoretical flow characteristics.



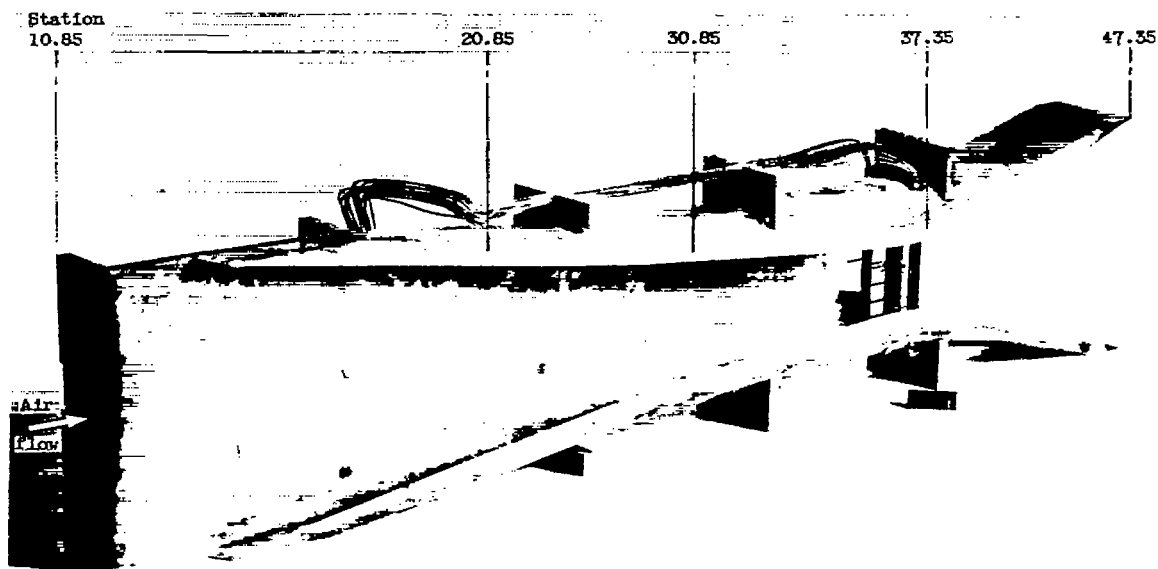
(b) Double-wedge inlet.

Figure 2. - Continued. Theoretical flow characteristics.



(c) 1.88-Isentropic inlet.

Figure 2. - Concluded. Theoretical flow characteristics.



C-36840

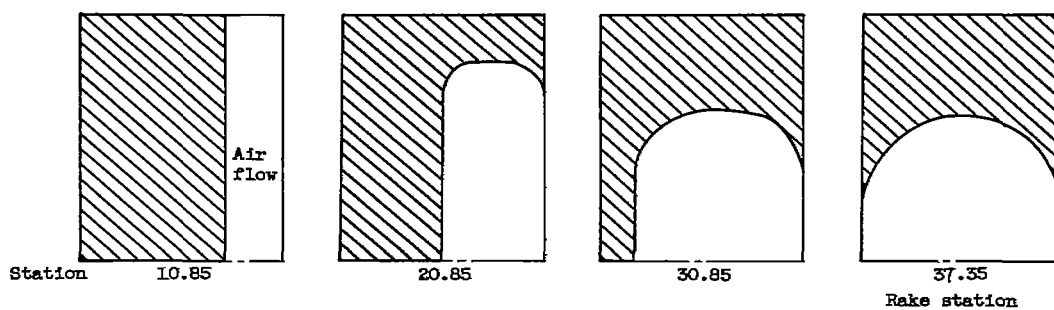
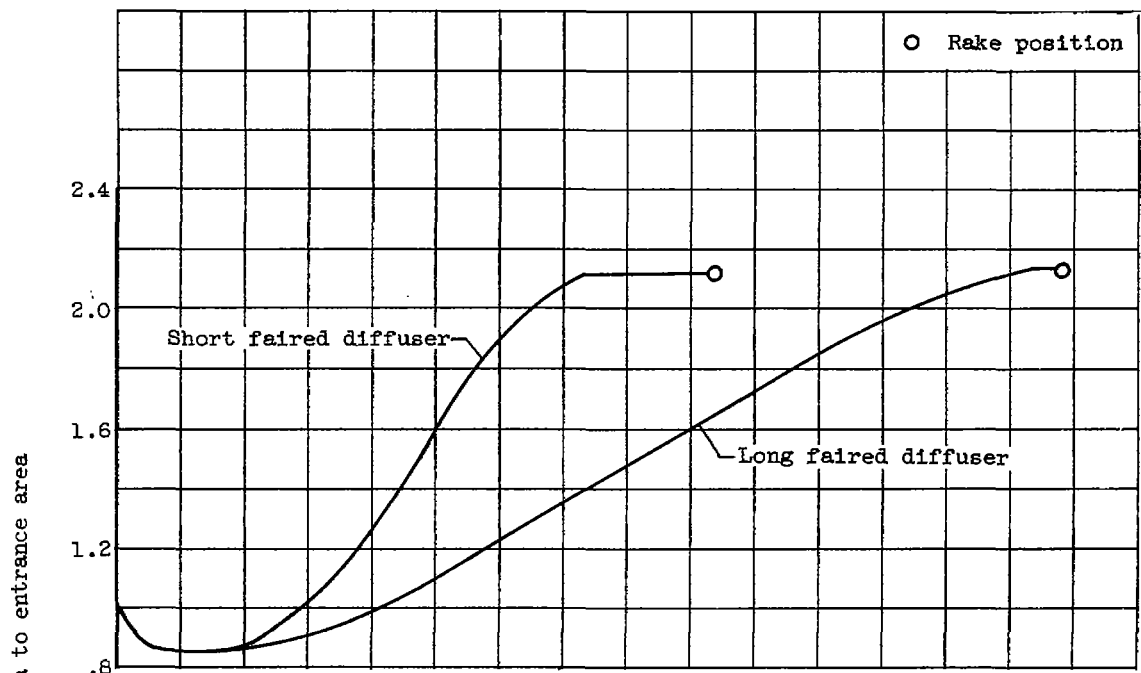
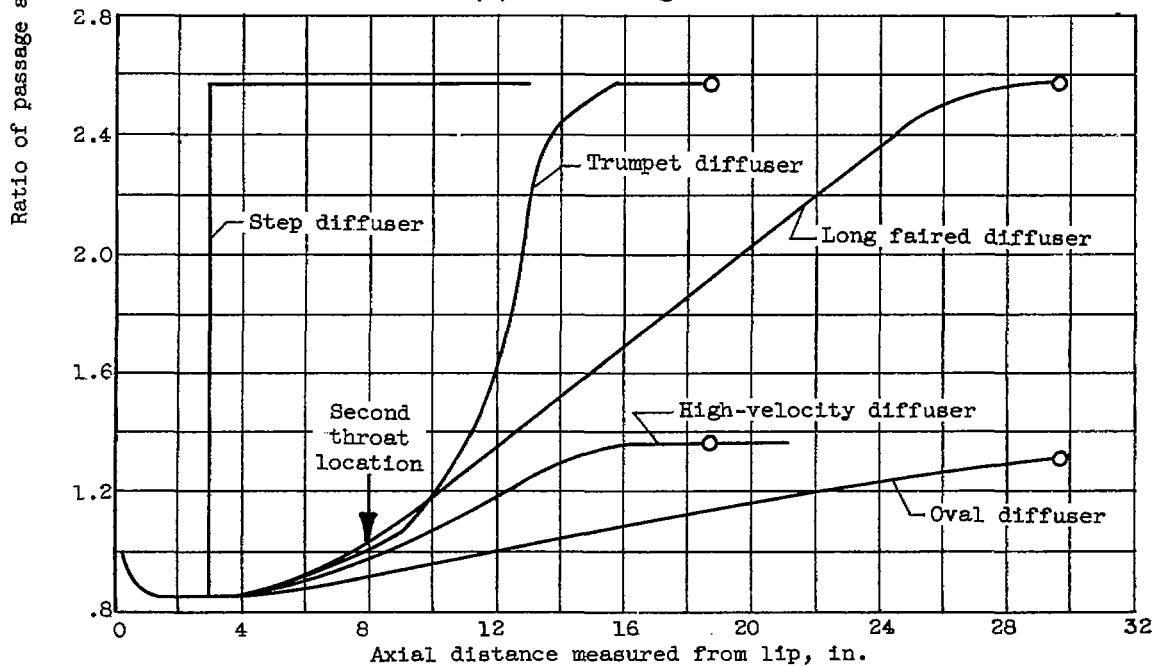


Figure 3. - Oval diffuser. (Stations measured in inches from leading edge of rectangular side plates.)



(a) Double-wedge inlet.



(b) 1.88-Isentropic inlet.

Figure 4. - Area variation of internal passage of inlets.

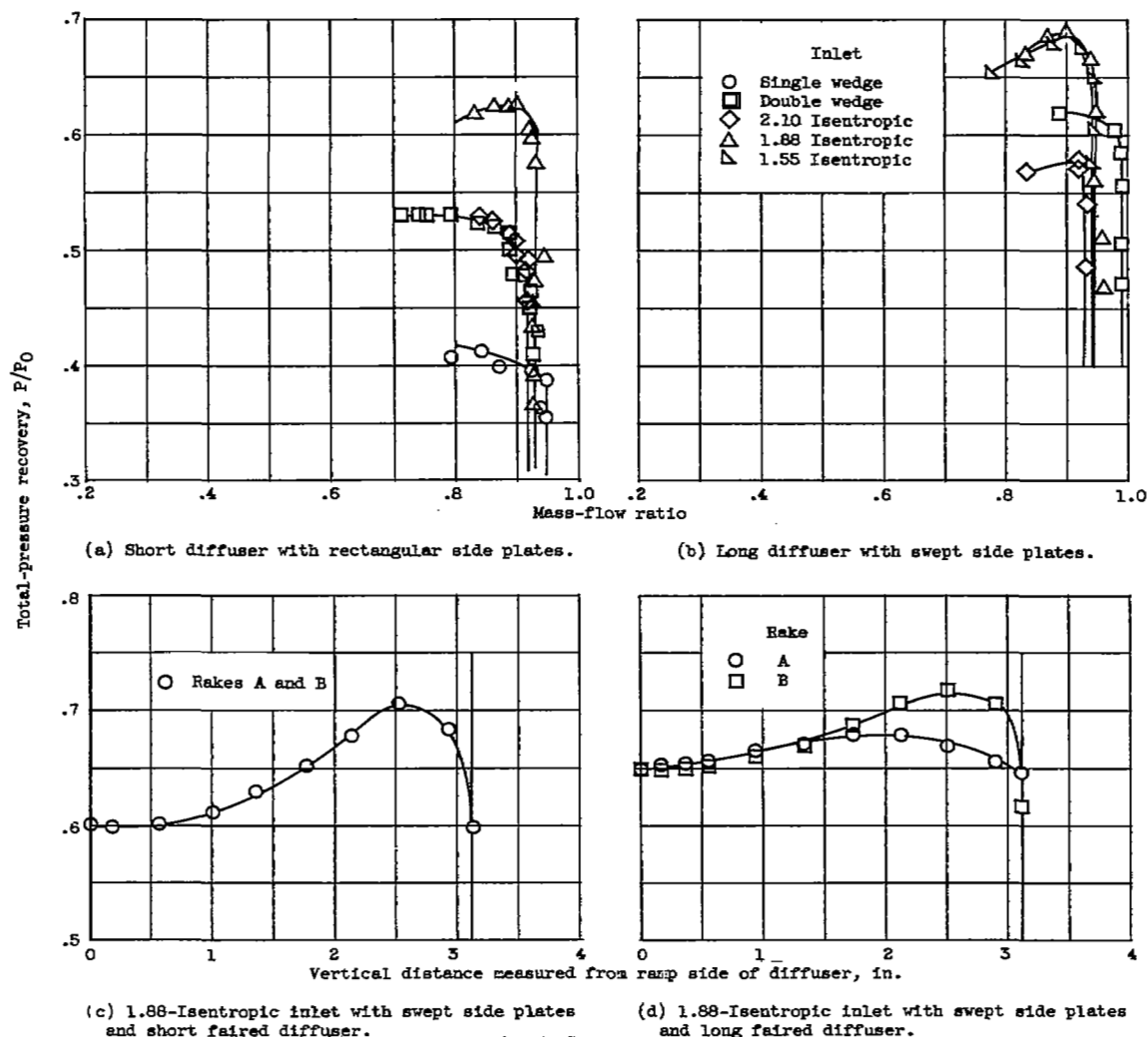
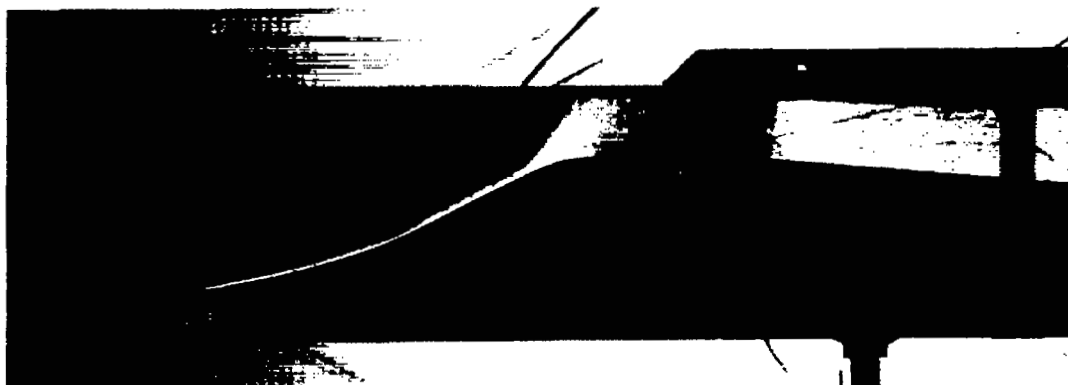
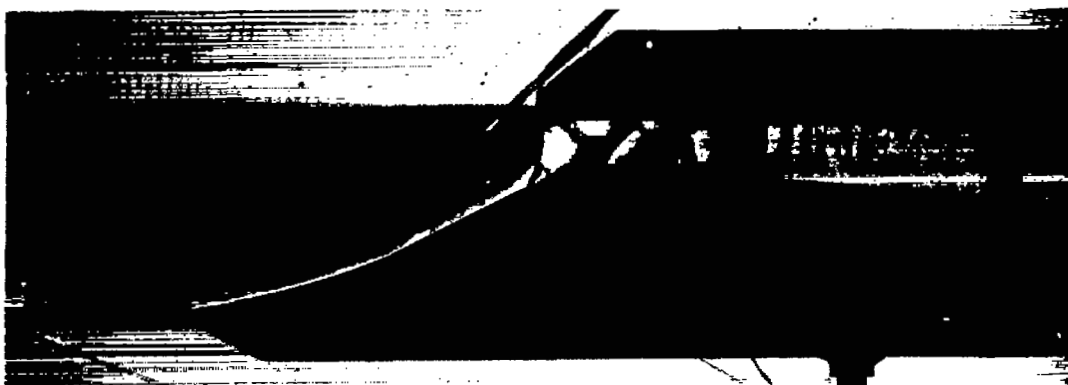


Figure 5. - Effect of compression surface on performance of various two-dimensional inlets at Mach number of approximately 3.1.



(a) 1.88-Isentropic wedge; no cowl.



(b) 1.88-Isentropic wedge; mass-flow ratio, 0.925; pressure recovery, 0.60.



(c) Double-wedge inlet; mass-flow ratio, 0.99; pressure recovery, 0.55.

Figure 6. - Schlieren photographs of two-dimensional inlet at free-stream Mach number 3.05.



(a) 0.012 Second.



(b) 0.030 Second.



(c) 0.033 Second.



(d) 0.037 Second.



(e) 0.040 Second.



(f) 0.042 Second.

C-40413

Figure 7. - Schlieren photographs of 2.10-isentropic inlet during inlet buzz at free-stream Mach number 3.12. (The times indicated are measured from an approximate beginning of buzz cycle.)



(a) Single-wedge inlet; slightly oscillating bow shock; mass-flow ratio, 0.72; pressure recovery, 0.38.



(b) Single-wedge inlet; slightly oscillating bow shock; mass-flow ratio, 0.77; pressure recovery, 0.38.



(c) Double-wedge inlet; steady bow shock; mass-flow ratio, 0.84; pressure recovery, 0.59.



(d) 2.10-Isentropic inlet with long faired diffuser; slightly oscillating bow shock; mass-flow ratio, 0.77; pressure recovery, 0.54.



(e) 1.88-Isentropic inlet with throat-constrictor diffuser; steady bow shock; mass-flow ratio, 0.46; pressure recovery, 0.62.

Figure 8. - Schlieren photographs of interaction of bow shock with boundary layer.



(a) Supercritical flow; mass-flow ratio, 0.99; pressure recovery, 0.36.



(b) Critical flow; mass-flow ratio, 0.98; pressure recovery, 0.39.



(c) Subcritical flow; steady bow shock; mass-flow ratio, 0.92; pressure recovery, 0.40.



(d) Subcritical flow; slightly oscillating bow shock; mass-flow ratio, 0.82, pressure recovery, 0.41.

Figure 9. - Schlieren photographs of single-wedge inlet with short diffusers at free-stream Mach number 3.12.

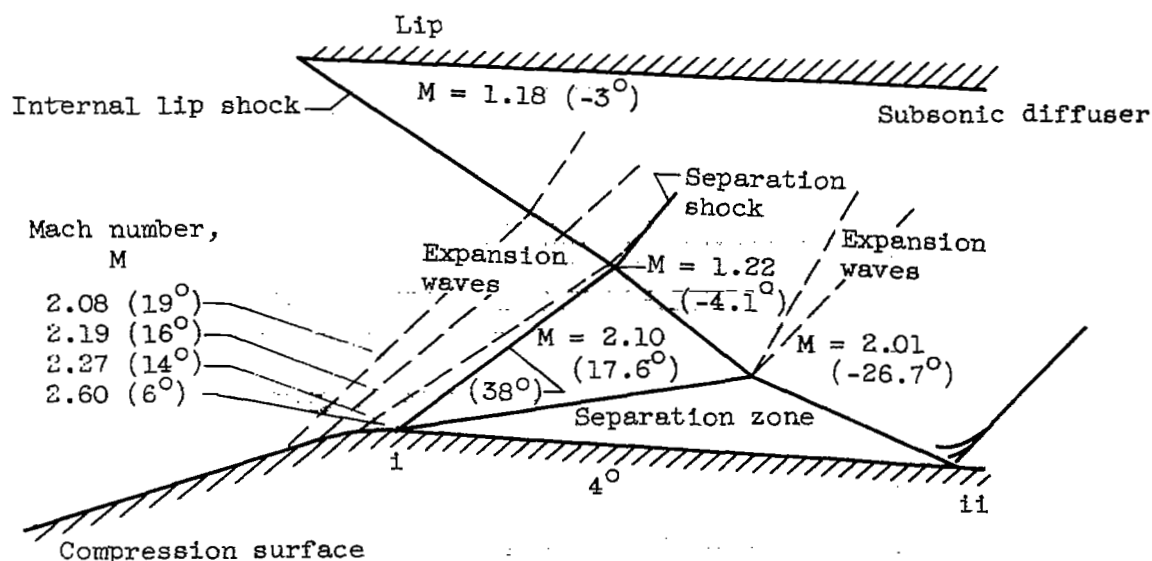
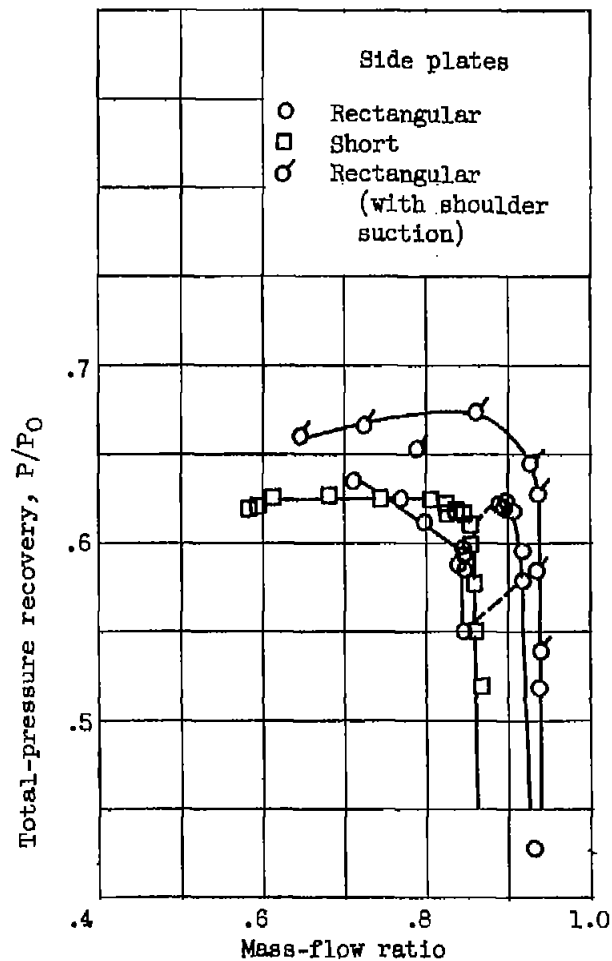
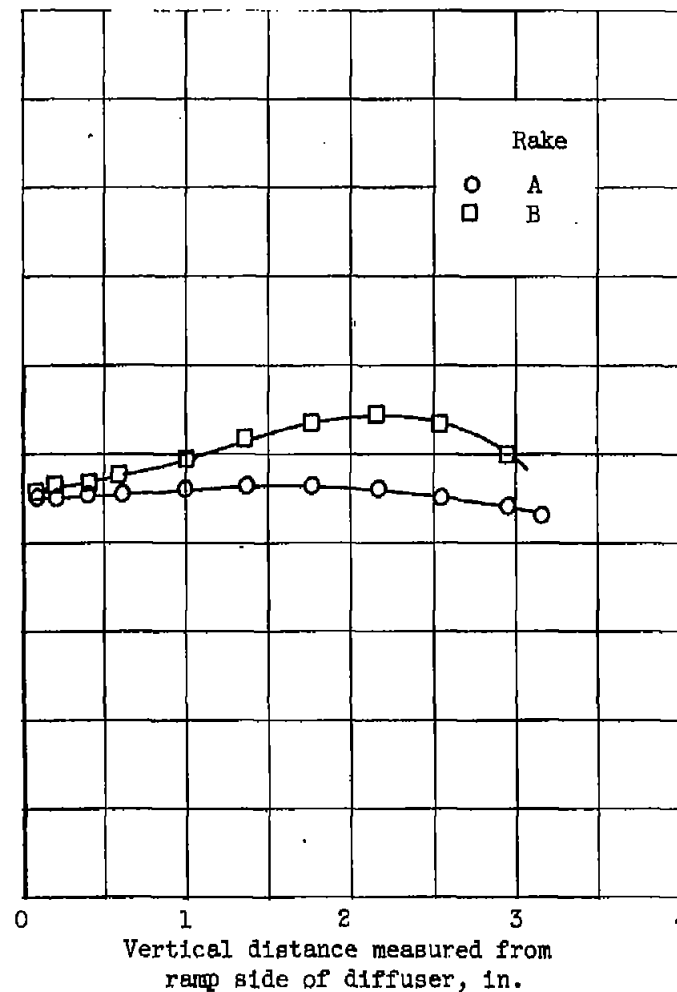


Figure 10. - Schematic drawing of calculated boundary-layer separation in single-wedge inlet. (Angles are measured from the horizontal; point of boundary-layer separation, i; point of boundary-layer reattachment, ii.)



(a) Effect of suction and side plates on pressure recovery.



(b) Total-pressure profiles with rectangular side plates and shoulder suction.

Figure 11. - Pressure characteristics of 1.55-isentropic inlet with long faired diffuser.



(a) Slightly supercritical flow; steady bow shock; mass-flow ratio, 0.89; pressure recovery, 0.62; no throat suction.



(b) Slightly supercritical flow; steady bow shock; mass-flow ratio, 0.84; pressure recovery, 0.59; no throat suction.



(c) Stable subcritical flow; mass-flow ratio, 0.71; pressure recovery, 0.64; no throat suction.

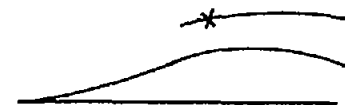


(d) Slightly subcritical flow; mass-flow ratio, 0.93; pressure recovery, 0.64; throat suction.

Figure 12. - Schlieren photographs of 1.55-isentropic inlet at free-stream Mach number 3.05.



(a) Supercritical flow; mass-flow ratio, 0.96; pressure recovery, 0.46.



Schematic sketch indicating point of separation on cowl lip for supercritical flow. See photograph.

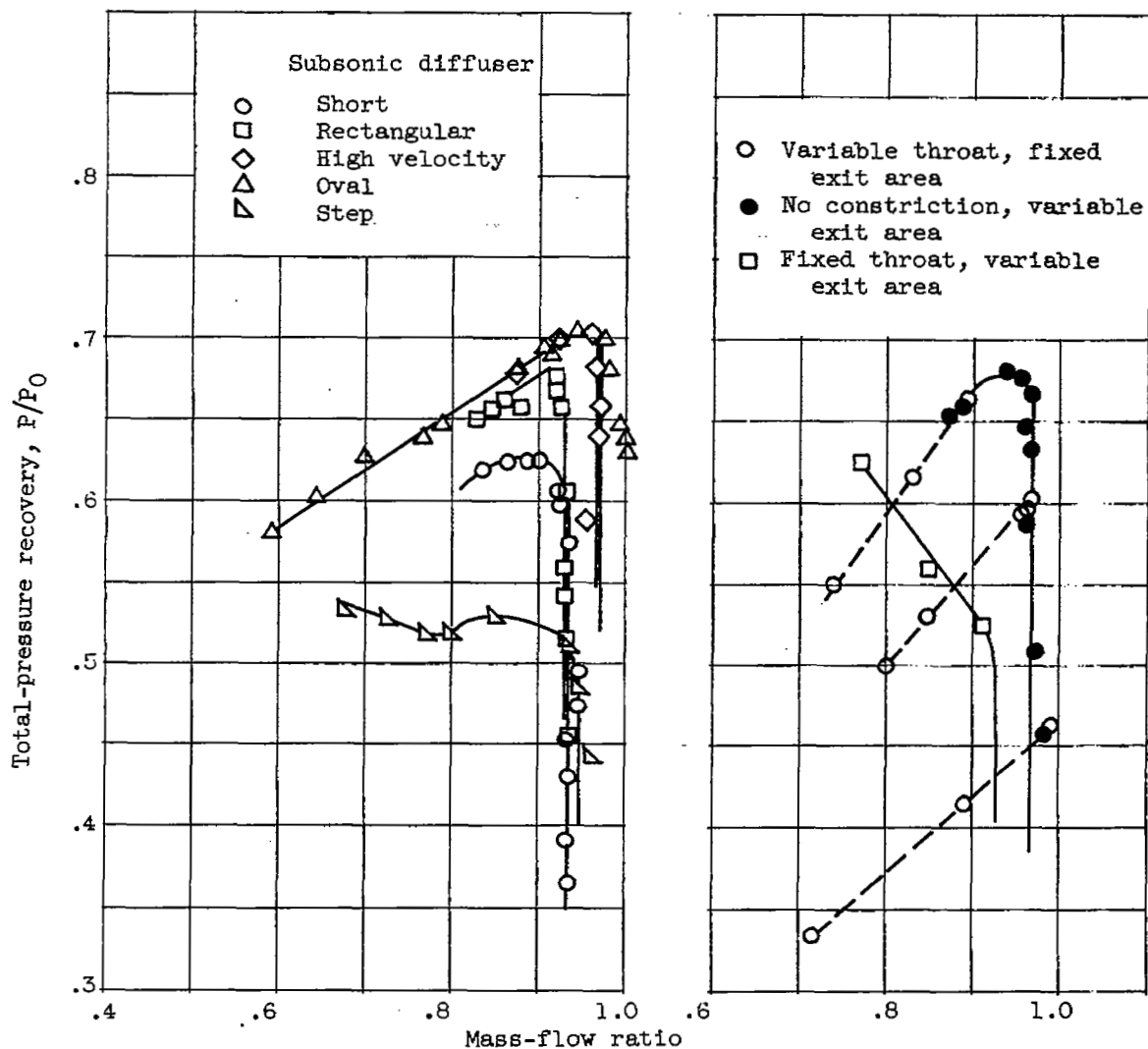


(b) Slightly subcritical flow; mass-flow ratio, 0.93; pressure recovery, 0.57.



Schematic sketch indicating oscillation of point of separation on cowl lip during slightly subcritical flow. See photograph.

Figure 13. - Schlieren photographs of 1.88-isentropic inlet with leading-edge roughness and special cowl.

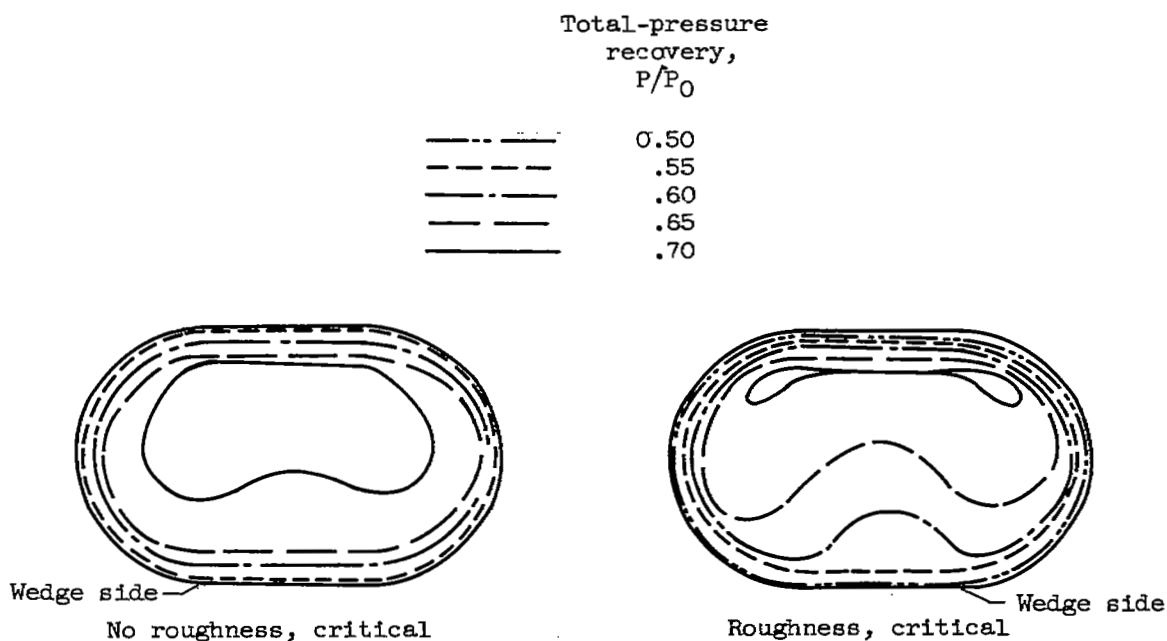


(a) Various fixed-geometry subsonic diffusers with rectangular side plates.

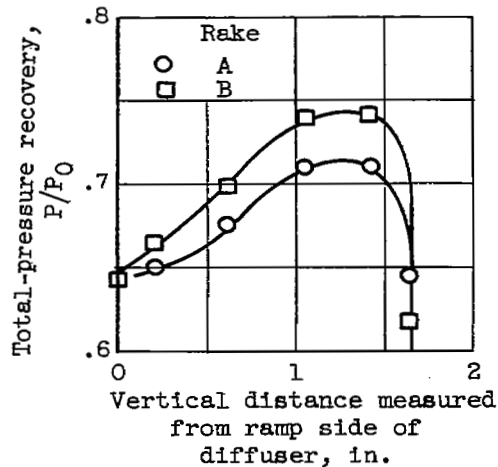
(b) Second-throat subsonic diffuser with rectangular side plates.

Figure 14. - Effect of subsonic diffuser on performance of 1.88-isentropic inlet at Mach number of approximately 3.1.

3730



(c) Pressure distributions at rake station for oval subsonic diffuser with rectangular side plates.



(d) Pressure profiles at rake station for high-velocity diffuser with swept side plates.

Figure 14. - Concluded. Effect of subsonic diffuser on performance of 1.88-isentropic inlet at Mach number of approximately 3.1.

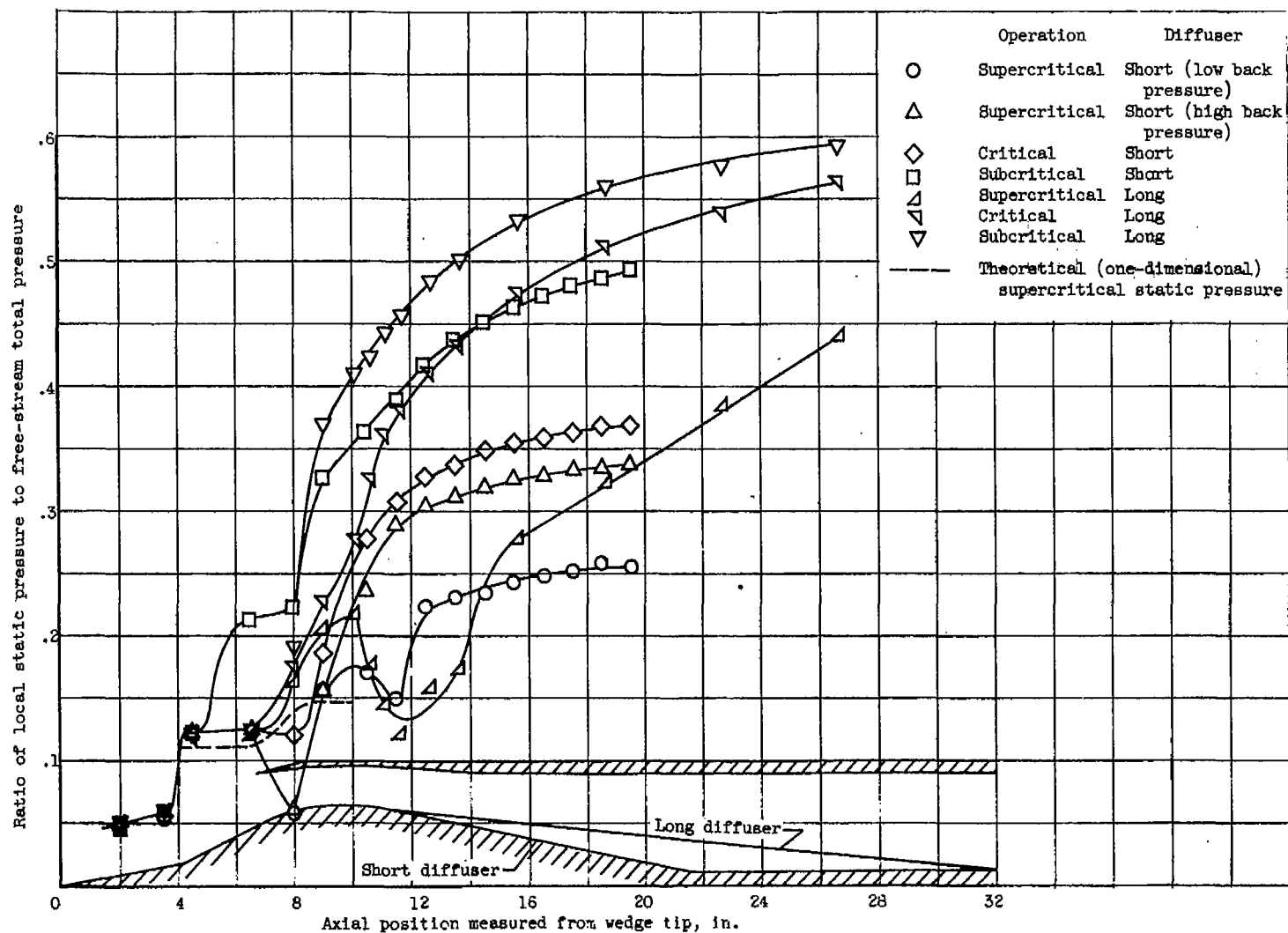
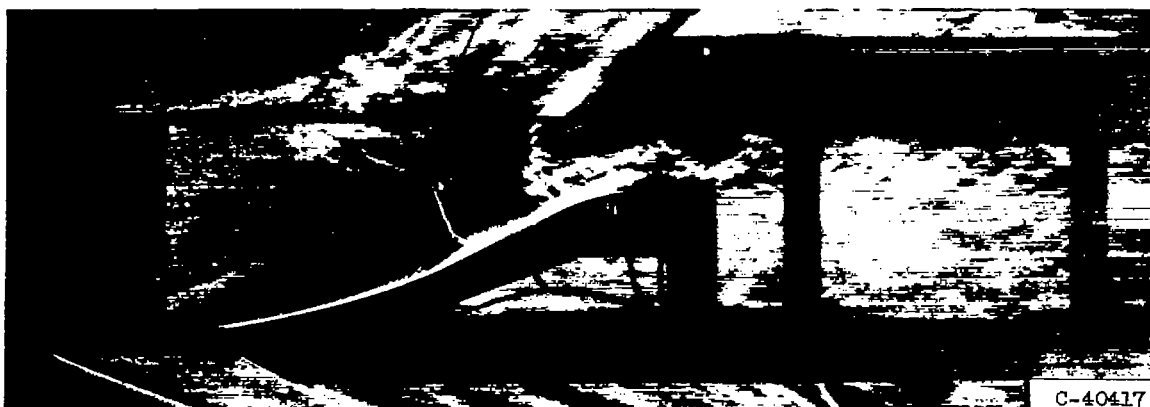


Figure 15. - Static pressure along wedge side of double-wedge inlet.



Critical flow; mass-flow ratio, 0.93; pressure recovery, 0.44.



Stable subcritical flow; mass-flow ratio, 0.68; pressure recovery, 0.53.

(a) Step diffuser.

Figure 16. - Schlieren photographs of 1.88-isentropic inlet at free-stream Mach number 3.05.



Mass-flow ratio, 0.97; pressure recovery, 0.46.



Mass-flow ratio, 0.97; pressure recovery, 0.46.



Steady bow shock; mass-flow ratio, 0.89; pressure recovery, 0.45.



C-40418

Steady bow shock; mass-flow ratio, 0.72; pressure recovery, 0.335.

(b) Second-throat diffuser.

Figure 16. - Concluded. Schlieren photographs of 1.88-isentropic inlet at free-stream Mach number 3.05.

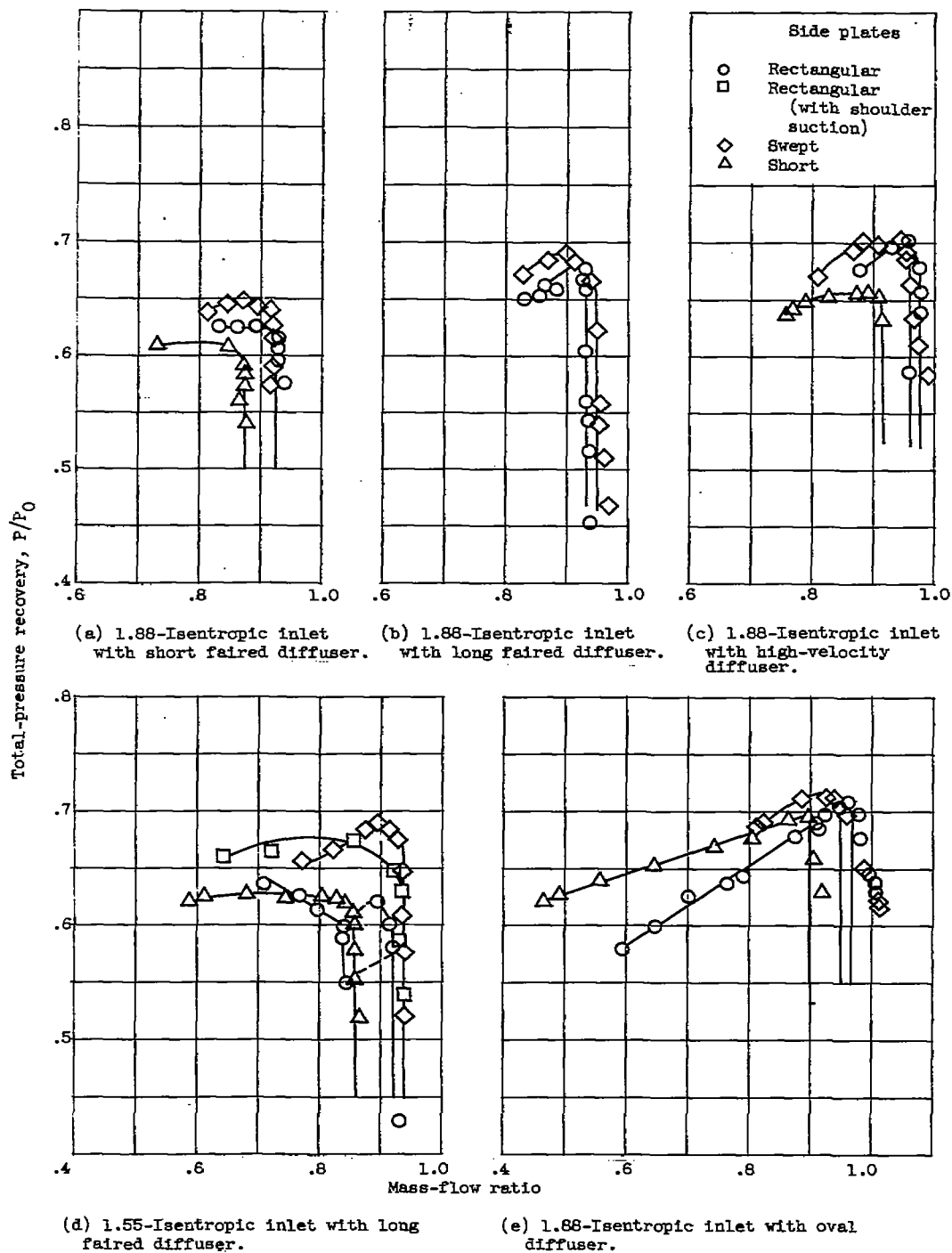


Figure 17. - Effect of side plate on performance of various two-dimensional inlets at Mach number of approximately 3.1.

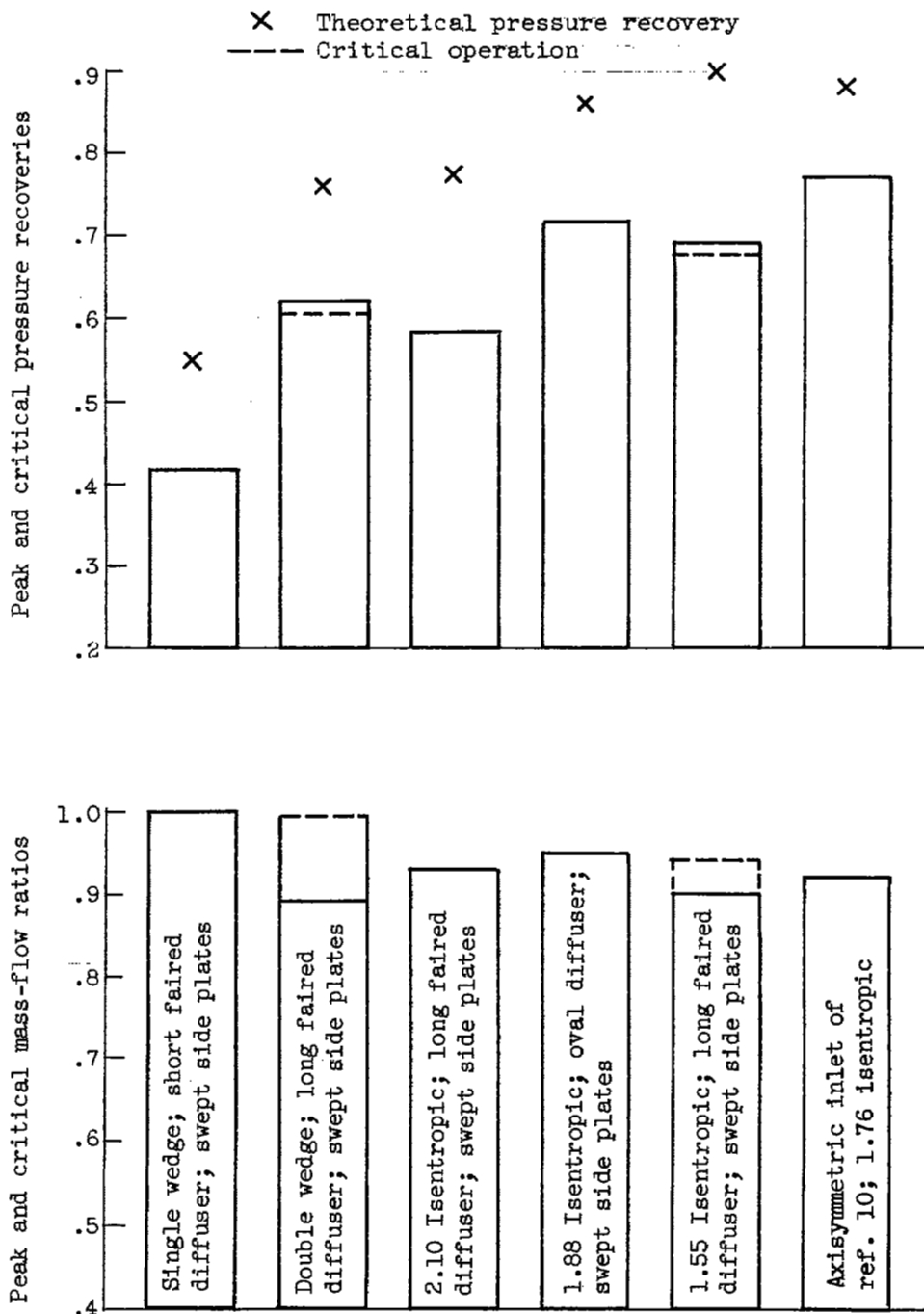


Figure 18. - Summary data for various inlets at free-stream Mach number 3.05.



3 1176 01436 5424

